

Distinct inactive conformations of the dopamine D₂ and D₃ receptors correspond to different extents of inverse agonism

J Robert Lane^{1,2*}, Ara M Abramyan³, Pramisha Adhikari³, Alastair C Keen^{1,2,4}, Kuo-Hao Lee³, Julie Sanchez^{1,2}, Ravi Kumar Verma³, Herman D Lim⁴, Hideaki Yano³, Jonathan A Javitch^{5,6,7*}, Lei Shi^{3*}

¹Division of Pharmacology, Physiology and Neuroscience, School of Life Sciences, Queen's Medical Centre, University of Nottingham, Nottingham, United Kingdom; ²Centre of Membrane Protein and Receptors, Universities of Birmingham and Nottingham, Nottingham, United Kingdom; ³Computational Chemistry and Molecular Biophysics Unit, National Institute on Drug Abuse - Intramural Research Program, National Institutes of Health, Baltimore, United States; ⁴Drug Discovery Biology, Department of Pharmacology and Medicinal Chemistry, Monash Institute of Pharmaceutical Sciences, Monash University, Parkville, Australia; ⁵Department of Psychiatry, Vagelos College of Physicians and Surgeons, Columbia University, New York, United States; ⁶Division of Molecular Therapeutics, New York State Psychiatric Institute, New York, United States; ⁷Department of Pharmacology, Vagelos College of Physicians and Surgeons, Columbia University, New York, United States

***For correspondence:**

Rob.Lane@nottingham.ac.uk (JRL);
jaj2@cumc.columbia.edu (JAJ);
lei.shi2@nih.gov (LS)

Competing interests: The authors declare that no competing interests exist.


Funding: See page 23

Received: 25 September 2019

Accepted: 24 January 2020

Published: 27 January 2020

Reviewing editor: Yibing Shan, DE Shaw Research, United States

 This is an open-access article, free of all copyright, and may be freely reproduced, distributed, transmitted, modified, built upon, or otherwise used by anyone for any lawful purpose. The work is made available under the [Creative Commons CC0 public domain dedication](https://creativecommons.org/licenses/by/4.0/).

Abstract By analyzing and simulating inactive conformations of the highly homologous dopamine D₂ and D₃ receptors (D₂R and D₃R), we find that eticlopride binds D₂R in a pose very similar to that in the D₃R/eticlopride structure but incompatible with the D₂R/risperidone structure. In addition, risperidone occupies a sub-pocket near the Na⁺ binding site, whereas eticlopride does not. Based on these findings and our experimental results, we propose that the divergent receptor conformations stabilized by Na⁺-sensitive eticlopride and Na⁺-insensitive risperidone correspond to different degrees of inverse agonism. Moreover, our simulations reveal that the extracellular loops are highly dynamic, with spontaneous transitions of extracellular loop 2 from the helical conformation in the D₂R/risperidone structure to an extended conformation similar to that in the D₃R/eticlopride structure. Our results reveal previously unappreciated diversity and dynamics in the inactive conformations of D₂R. These findings are critical for rational drug discovery, as limiting a virtual screen to a single conformation will miss relevant ligands.

Introduction

G-protein-coupled receptors (GPCRs) are important therapeutic targets for numerous human diseases. Our understanding of GPCR functional mechanisms has evolved from a simple demarcation of single active and inactive states to the appreciation and detection of multiple active states responsible for partial or biased agonism (Latorraca et al., 2017; Venkatakrishnan et al., 2013; Weis and Kobilka, 2018). High-resolution crystal structures of these proteins are vital for structure-based (rational) drug discovery (RDD) efforts designed to tailor selectivity and efficacy (Congreve et al., 2014; Michino et al., 2015a). While considerable efforts have been directed at

eLife digest Almost a third of prescribed drugs work by acting on a group of proteins known as GPCRs (short for G-protein coupled receptors), which help to transmit messages across the cell's outer barrier. The neurotransmitter dopamine, for instance, can act in the brain and body by attaching to dopamine receptors, a sub-family of GPCRs. The binding process changes the three-dimensional structure (or conformation) of the receptor from an inactive to active state, triggering a series of molecular events in the cell.

However, GPCRs do not have a single 'on' or 'off' state; they can adopt different active shapes depending on the activating molecule they bind to, and this influences the type of molecular cascade that will take place in the cell. Some evidence also shows that classes of GPCRs can have different inactive structures; whether this is also the case for the dopamine D₂ and D₃ receptors remained unclear. Mapping out inactive conformations of receptors is important for drug discovery, as compounds called antagonists can bind to inactive receptors and interfere with their activation.

Lane et al. proposed that different types of antagonists could prefer specific types of inactive conformations of the dopamine D₂ and D₃ receptors. Based on the structures of these two receptors, the conformations of D₂ bound with the drugs risperidone and eticlopride (two dopamine antagonists) were simulated and compared. The results show that the inactive conformations of D₂ were very different when it was bound to eticlopride as opposed to risperidone. In addition D₂ and D₃ showed a very similar conformation when attached to eticlopride. The two drugs also bound to the inactive receptors in overlapping but different locations. These computational findings, together with experimental validations, suggest that D₂ and D₃ exist in several inactive states that only allow the binding of specific drugs; these states could also reflect different degrees of inactivation. Overall, the work by Lane et al. contributes to a more refined understanding of the complex conformations of GPCRs, which could be helpful to screen and develop better drugs.

the development of biased agonists that couple preferentially to a particular effector pathway (*Free et al., 2014; Manglik et al., 2016; McCorvy et al., 2018*), less attention has been dedicated to the possibility that different antagonist scaffolds with differing efficacy of inverse agonism might lead to different receptor conformations and hence different 'inactive' states. Such a possibility could have a major impact on RDD for antagonists, since a GPCR crystal structure stabilized by a particular antagonist might represent an invalid docking target for an antagonist that prefers a different inactive conformation. Although substantial differences in antagonist binding mode and position of the binding pockets have been revealed among different aminergic receptors, no conformational differences has been detected for the inactive state in any individual aminergic receptor (*Michino et al., 2015a*). In particular, although a number of antagonists derived from different scaffolds have been co-crystallized with the β_2 adrenergic receptor, conformational differences among these crystal structures are minimal (*Michino et al., 2015a*).

Curiously, the inactive state structures of the highly homologous dopamine D₂ and D₃ receptors (D₂R and D₃R) revealed substantial differences on the extracellular side of the transmembrane domain, especially in TM6 (*Figure 1*), when bound with antagonists derived from different scaffolds (*Chien et al., 2010; Wang et al., 2018*). Specifically, the D₃R structure is in complex with eticlopride, a substituted benzamide (PDB: 3PBL) (*Chien et al., 2010*), while the D₂R structure is bound with risperidone, a benzisoxazole derivative (PDB: 6CM4) (*Wang et al., 2018*). The binding poses of the two ligands differ substantially. Risperidone is oriented relatively perpendicular to the membrane plane with its benzisoxazole ring penetrating into a hydrophobic pocket beneath the orthosteric binding site (OBS) of D₂R; in contrast, eticlopride is oriented relatively parallel to the membrane plane and contacts the extracellular portion of TM5 in D₃R, a sub-pocket that risperidone does not occupy in D₂R (*Sibley and Shi, 2018; Wang et al., 2018*). Nemonapride, another substituted benzamide, binds in the OBS of the slightly divergent D₄R (PDB: 5WIV) (*Wang et al., 2017*) in a manner very similar to that of eticlopride in the D₃R (*Sibley and Shi, 2018*).

Importantly, the co-crystallized ligands (risperidone, eticlopride, and nemonapride) display little subtype selectivity across D₂R, D₃R, and D₄R (*Chien et al., 2010; Hirose and Kikuchi, 2005; Silvestre and Prous, 2005; Wang et al., 2017*) (also see PDSP database; *Roth et al., 2000*). Given

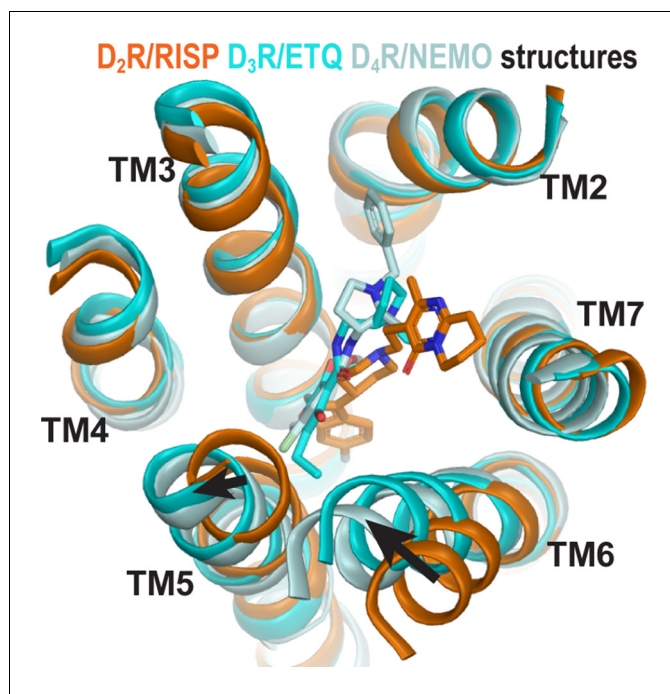


Figure 1. The structures of homologous D₂R, D₃R, and D₄R show different conformations in the extracellular vestibules. Superpositioning of D₂R, D₃R, and D₄R structures shows that the binding of eticlopride (ETQ, cyan) in D₃R and nemonapride (NEMO, pale cyan) in D₄R result in outward and inward rearrangements of the extracellular portions of TM5 and TM6, respectively, compared to the binding of risperidone (RISP, orange) in D₂R. The online version of this article includes the following figure supplement(s) for figure 1:

Figure supplement 1. Chemical structure alignments of the non-selective D₂-like receptors ligands.

the high homology among these D₂-like receptors, especially between D₂R and D₃R, the drastic conformational differences between the inactive state structures of these receptors may be better explained by different binding poses of antagonists bearing different scaffolds rather than inherent differences in the receptors. Thus, we hypothesized that different antagonist scaffolds may favor distinct inactive conformations of D₂R. To test this hypothesis, we carried out extensive molecular dynamics (MD) simulations of D₂R in complex with non-selective antagonists derived from different scaffolds to characterize the plasticity of the OBS and the extracellular loop dynamics in the inactive conformational state.

Results

The Ile^{3.40} sub-pocket is occupied by risperidone and spiperone but not eticlopride in D₂R

Compared to eticlopride bound in the D₃R structure, risperidone in the D₂R structure penetrates deeper into the binding site, with its benzisoxazole moiety occupying a sub-pocket that eticlopride does not reach. By examining the D₂R/risperidone structure, we found that the benzisoxazole moiety is enclosed by eight residues in D₂R, which are identical among all D₂-like receptors (i.e. D₂R, D₃R, and D₄R): Cys118^{3.36} (superscripts denote Ballesteros-Weinstein numbering *Ballesteros and Weinstein, 1995*), Thr119^{3.37}, Ile122^{3.40}, Ser197^{5.46}, Phe198^{5.47}, Phe382^{6.44}, Trp386^{6.48}, and Phe390^{6.52}. Notably, three of these residues (Ile122^{3.40}, Phe198^{5.47}, and Phe382^{6.44}) on the intracellular side of the OBS that we previously defined (*Michino et al., 2015a*), accommodate the F-substitution at the tip of the benzisoxazole ring in a small cavity (termed herein as the Ile^{3.40} sub-pocket) (*Figure 2a*). Both Ile122^{3.40} and Phe382^{6.44} of this Ile^{3.40} sub-pocket are part of the conserved Pro^{5.50}-Ile^{3.40}-Phe^{6.44} motif that undergoes rearrangement upon receptor activation (*Rasmussen et al., 2011*), and

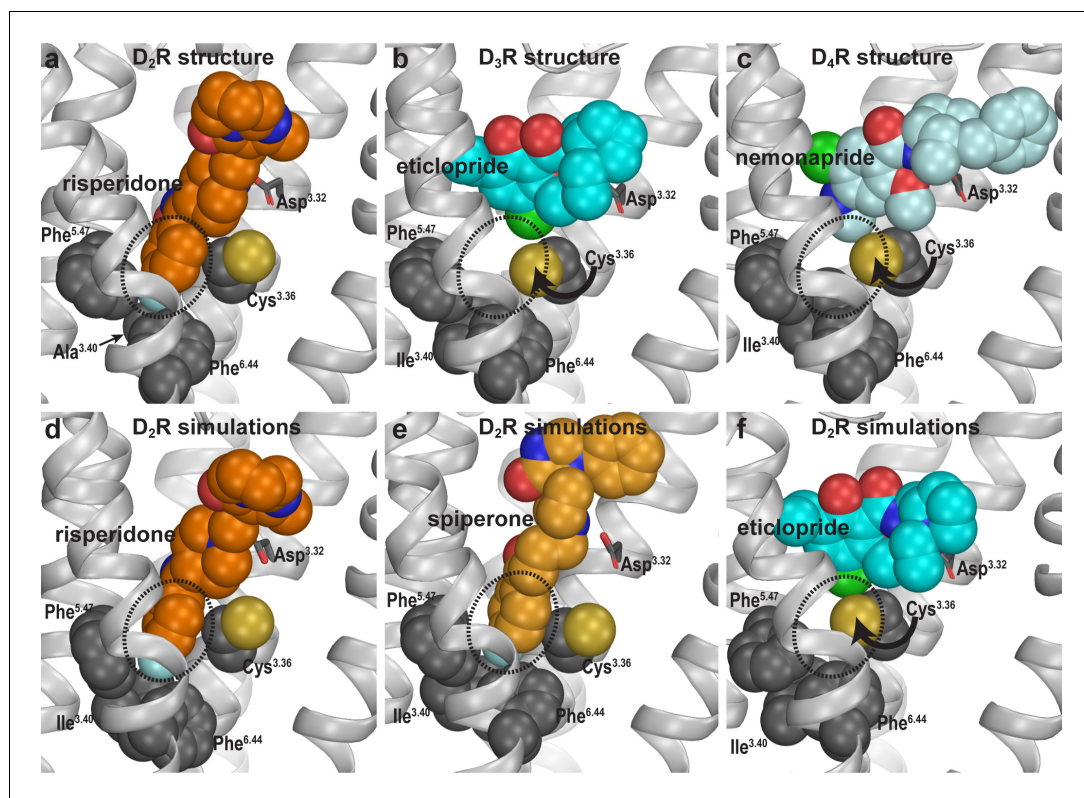


Figure 2. Divergent occupations of the Ile^{3.40} sub-pocket by non-selective ligands from different scaffolds. In the D₂R structure (a), the F-substitution on the benzisoxazole ring of risperidone occupies the Ile^{3.40} sub-pocket (dotted circle) enclosed by conserved Ile^{3.40} (mutated to Ala in the crystal structure to thermostabilize the receptor), Phe^{5.47}, and Phe^{6.44}. The same viewing angle shows that in the D₃R (b) and D₄R (c) structures, Cys^{3.36} rotates to fill in the Ile^{3.40} sub-pocket, and the substituted benzamides eticlopride and nemonapride cannot occupy the aligned sub-pockets. In our D₂R/risperidone simulations (d), risperidone maintains its pose revealed by the crystal structure. In the D₂R/spiperone simulations (e), the Ile^{3.40} sub-pocket is similarly occupied as in D₂R/risperidone. In the D₂R/eticlopride simulations (f), the Ile^{3.40} sub-pocket is collapsed as in the D₃R (b) and D₄R (c) structures (this trend is independent of the force field being used in the simulations).

The online version of this article includes the following figure supplement(s) for figure 2:

Figure supplement 1. Allosteric communication between the Ile^{3.40} sub-pocket and the Na⁺ binding site.

we have found that the I122^{3.40}A mutation renders D₂R non-functional (Klein Herenbrink *et al.*, 2019; Wang *et al.*, 2018). Interestingly, this Ile^{3.40} sub-pocket is collapsed in both the D₃R and D₄R structures (Sibley and Shi, 2018; Figure 2b,c). We noted that this collapse is associated with rotation of the sidechain of Cys^{3.36}: In the D₂R/risperidone structure, the sidechain of Cys^{3.36} faces the OBS, whereas in the D₃R/eticlopride and D₄R/nemonapride structures, it rotates downwards to partially fill the Ile^{3.40} sub-pocket (Figure 2a–c).

To test our hypothesis that these observed differences in the crystal structures are due to the binding of antagonists bearing different scaffolds but not intrinsic divergence of D₂-like receptors, we compared the binding modes of three non-selective antagonists in D₂R. We reverted three thermostabilizing mutations introduced for crystallography (I122^{3.40}A, L375^{6.37}A, and L379^{6.41}A) back to their WT residues, established WT D₂R models in complex with risperidone, spiperone, or eticlopride, and carried out extensive MD simulations (see Materials and methods, Figure 1—figure supplement 1 and Table 1).

In our prolonged MD simulations of the WT D₂R/risperidone complex (>65 μs, Table 1), we observed that risperidone stably maintains the binding pose captured in the crystal structure, even without the thermostabilizing mutations (Figure 2d). Thus, the I122^{3.40}A mutation has minimal impact on the binding pose of risperidone. Interestingly, in the simulations of the WT D₂R model in

Table 1. Summary of molecular dynamics simulations.

Receptor	Ligand	Bound Na^+	Number of OPLS3e trajectories	Number of CHARMM36 trajectories	Accumulated simulation time (ns)
D ₂ R	Risperidone	+	12		28410
		-	11		42240
	Spiperone	+	22		42000
		-	17		29550
	Eticlopride	+	5	12	51540
		-	7		11280
	(-)-Sulpiride	+	3		4500
		-	3		3600
Aripiprazole	+	40		66660	
D ₃ R	Eticlopride	+		3	13200
		-		4	6240
	R22	+		7	33600
	S22	-		7	59400
Total			120	33	392220

complex with spiperone, a butyrophenone derivative, the F-substitution on the butyrophenone ring similarly occupies the Ile^{3.40} sub-pocket as risperidone (**Figure 2e**). Note that the F-substitutions in risperidone and spiperone are located at similar distances to the protonated N atoms that interact with Asp^{3.32} (measured by the number of carbon atoms between them, **Figure 1—figure supplement 1**) and these two ligands appear to be optimized to occupy the Ile^{3.40} sub-pocket.

In contrast, in our simulations of the D₂R/eticlopride complex, the eticlopride pose revealed in the D₃R structure (PDB: 3PBL) is stable throughout the simulations and does not protrude into the Ile^{3.40} sub-pocket (**Figure 2f**). Consistent with the difference in the crystal structures noted above (**Figure 2a,b**), when risperidone and spiperone occupy the Ile^{3.40} sub-pocket, the sidechain of Cys118^{3.36} rotates away with its χ_1 rotamer in *gauche-*, while in the presence of the bound eticlopride, this rotamer is stable in *trans* (**Figure 2—figure supplement 1**).

To validate these computational findings regarding the occupation of the Ile^{3.40} sub-pocket, we mutated Ile122^{3.40} of WT D₂R to both Trp and Ala and characterized how these mutations affect the binding affinities for spiperone, risperidone, and eticlopride (**Table 2**). We hypothesized that the bulkier sidechain of Trp at position 3.40 would hamper the binding of spiperone and risperidone

Table 2. The effect of mutations on the binding affinities of selected D₂R ligands.

The affinities of [³H]spiperone were determined in saturation experiments at WT or mutant SNAP-tagged D₂₅R_s stably expressed in FlpIn CHO cells. Binding affinity values for risperidone and eticlopride were obtained in competition binding experiments. Means of *n* independent experiments performed in triplicate are shown with 95% confidence intervals.

SNAP-D ₂₅ R	[³ H]spiperone saturation binding		[³ H]spiperone competition binding			
	pK_d (K_d , nM) (95% CI)	N	Risperidone pK_i (K_i , nM) (95% CI)	N	Eticlopride pK_i (K_i , nM) (95% CI)	N
WT	9.74 (0.18) (9.36–10.14)	3	8.55 (2.8) (8.07–9.04)	8	9.84 (0.14) (9.10–10.58)	3
WT -Na ⁺	9.70 (0.20) (9.09–10.32)	3	8.96 (1.1) (8.84–9.08)	6	-	
I122 ^{3.40} A	9.74 (0.18) (9.09–10.38)	3	8.14 (7.9) (7.97–8.32)	8	10.33 (0.04) (10.22–10.44)	3
I122 ^{3.40} W	8.95 (1.15) (8.59–9.30)	3	7.43 (37) (7.11–7.75)	5	9.61 (0.25) (9.33–9.89)	4

since they occupy the Ile^{3.40} sub-pocket but have no effect on eticlopride binding, while the smaller Ala should not affect the binding of spiperone or risperidone. Consistent with this hypothesis, the I122W mutation decreased the binding affinities of risperidone (13-fold) and spiperone (6-fold) compared to WT but had no effect on that of eticlopride. In contrast, the I122A mutation did not affect the affinities of spiperone or risperidone, which is consistent with our simulation results that show the I122A mutation has minimal impact on risperidone binding. In contrast, I122A caused a threefold increase in the affinity of eticlopride, suggesting that the I122A mutation may promote an inactive conformation of D₂R that favors eticlopride binding. Together these results support our proposal that different antagonist scaffolds may favor distinct inactive conformations of D₂R.

Occupation of the Ile^{3.40} sub-pocket confers insensitivity to Na⁺ in antagonist binding

Ligand binding in D₂-like receptors can be modulated by Na⁺ bound in a conserved allosteric binding pocket coordinated by Asp^{2.50} and Ser^{3.39} (Michino *et al.*, 2015b; Neve, 1991; Wang *et al.*, 2017). Note that the aforementioned Cys^{3.36} and Ile^{3.40} are adjacent to the Na⁺ coordinating Ser^{3.39}; thus, we further hypothesized that the occupation of the Ile^{3.40} sub-pocket by spiperone or risperidone makes them insensitive to Na⁺. To test this hypothesis, we simulated D₂R/risperidone, D₂R/spiperone, D₂R/eticlopride, and D₂R/(-)-sulpiride complexes in the presence versus absence of bound Na⁺ (Table 1). Interestingly, the occupancy of the Ile^{3.40} sub-pocket by either spiperone or risperidone was unaffected by the presence or absence of bound Na⁺ (Figure 2—figure supplement 1). In contrast, while the poses of eticlopride and (-)-sulpiride are highly stable in the presence of bound Na⁺, they oscillated between different poses in the absence of Na⁺. These oscillations are associated with the sidechain of Cys^{3.36} swinging back and forth between the two rotamers, suggesting an important role of Na⁺ binding in stabilizing the poses of eticlopride and (-)-sulpiride and the configuration of the Ile^{3.40} sub-pocket (Figure 2—figure supplement 1). Interestingly, the previous MD simulations described by Wang *et al.* indicated that nemonapride's binding pose in D₄R is more stable in the presence of bound Na⁺ as well (Wang *et al.*, 2017).

Consistent with these computational results, we have previously shown that spiperone binding is insensitive to the presence of Na⁺, while the affinities of eticlopride and sulpiride are increased in the presence of Na⁺ (Michino *et al.*, 2015b). In this study, we performed binding experiments in the absence or presence of Na⁺ and found the affinity of risperidone to be unaffected, in accordance with this hypothesis (Table 2).

Together these findings support our hypothesis that the ability of a ligand to bind the Ile^{3.40} sub-pocket relates with its sensitivity to Na⁺ in binding, due to allosteric connections between the sub-pocket and the Na⁺ binding site.

Functional consequences of distinct antagonist-bound inactive conformations

To further investigate the functional impact of these conformational differences surrounding the OBS, we used a bioluminescence resonance energy transfer (BRET) assay, which measures conformational changes of the Go protein heterotrimer following activation by D₂R (Michino *et al.*, 2017), to evaluate the inverse agonism activities of several representative D₂R ligands. These ligands can be categorized into two groups according to their sensitivities to Na⁺ in binding at D₂R, which have been characterized either in our current study or in previous studies (Michino *et al.*, 2015b; Neve, 1991; Newton *et al.*, 2016). While risperidone, spiperone, and (+)-butaclamol have been found to be insensitive to Na⁺ in binding, (-)-sulpiride, eticlopride, and raclopride show enhanced binding affinities in the presence of Na⁺. Using quinpirole as a reference full agonist, we found that the Na⁺ insensitive ligands display significantly greater inverse agonism (< -30% that of the maximal response of quinpirole) relative to the Na⁺-sensitive ligands (> -15% that of the maximal response of quinpirole, Figure 3). These observations are consistent with findings from earlier [³⁵S]GTPγS binding experiments of Roberts and Strange in which (+)-butaclamol, risperidone, and spiperone were found to inhibit significantly more [³⁵S]GTPγS binding than raclopride and (-)-sulpiride (Roberts and Strange, 2005). Of note, these [³⁵S]GTPγS-binding experiments were performed in the absence of Na⁺.

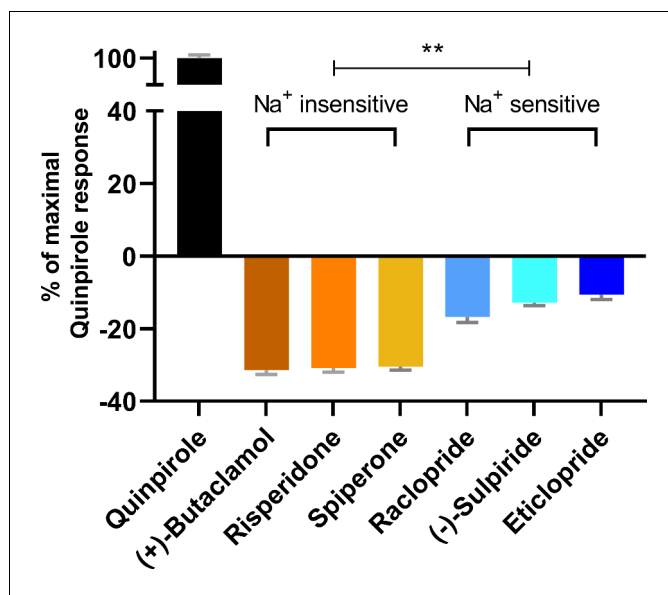


Figure 3. The extent of inverse agonism is negatively related with the Na⁺ sensitivity of ligand binding. In a D₂R-Go BRET assay, the maximal responses of the indicated ligands are normalized to that of the reference full agonist quinpirole. The ligands that are insensitive to Na⁺ in D₂R binding display significantly higher inverse agonism (in each case, **p<0.0001 using ordinary one-way ANOVA followed by Tukey's multiple comparisons test) than the Na⁺-sensitive ligands; however, within the Na⁺-sensitive group, raclopride is significantly different from eticlopride (p=0.005).

Based on these functional data together with the different binding modes revealed by our computational simulations, we propose that ligands that occupy the Ile^{3.40} sub-pocket exhibit a greater level of inverse agonism as compared to those that do not. Therefore, across the tested inverse agonists there is a negative relation between ligand sensitivity to Na⁺ and the extent of inverse agonism at D₂R. The differential occupation of the Ile^{3.40} sub-pocket is the structural basis for the Na⁺ sensitivity, which contributes significantly to the extent of inverse agonism of the tested ligands.

Plasticity of the ligand-binding site propagates to affect the overall receptor conformation

By occupying the Ile^{3.40} sub-pocket, the benzisoxazole moiety of risperidone pushes the conserved Phe^{6.52} away from the binding site in the D₂R/risperidone structure compared to its position in the D₃R/eticlopride structure. This interaction is responsible for positioning the aromatic cluster of TM6 and TM7 (Trp^{6.48}, Phe^{6.51}, Phe^{6.52}, His^{6.55}, and Tyr^{7.35}) in D₂R differently from its configurations in the D₃R and D₄R structures, resulting in an overall outward positioning of the extracellular portion of TM6 in D₂R (*Figure 4—figure supplement 1*). On the extracellular side of the OBS, the space near Ser^{5.42} and Ser^{5.43} that accommodates the bulky substitutions of the benzamide rings of the bound eticlopride and nemonapride in the D₃R and D₄R structures is not occupied by risperidone in D₂R, which is likely associated with the inward movement of the extracellular portion of TM5 in D₂R relative to those in the D₃R and D₄R structures (*Figure 1*).

To evaluate whether these conformational rearrangements are due to the minor divergence in these regions of the receptors or to the ligand-binding site plasticity that accommodates ligands bearing different scaffolds, we compared the resulting conformations of D₂R bound with risperidone or eticlopride. We observed the same trend of rearrangements of the transmembrane segments surrounding the OBS in the resulting receptor conformations from our D₂R/risperidone and D₂R/eticlopride simulations (*Figure 4a*), that is, an inward movement of TM6 and outward movement of TM5 in the presence of the bound eticlopride (*Figure 4b,c*). Without such movements in D₂R/eticlopride, Ser193^{5.42} and Ser194^{5.43} would clash with the bound eticlopride (*Figure 4a*). These

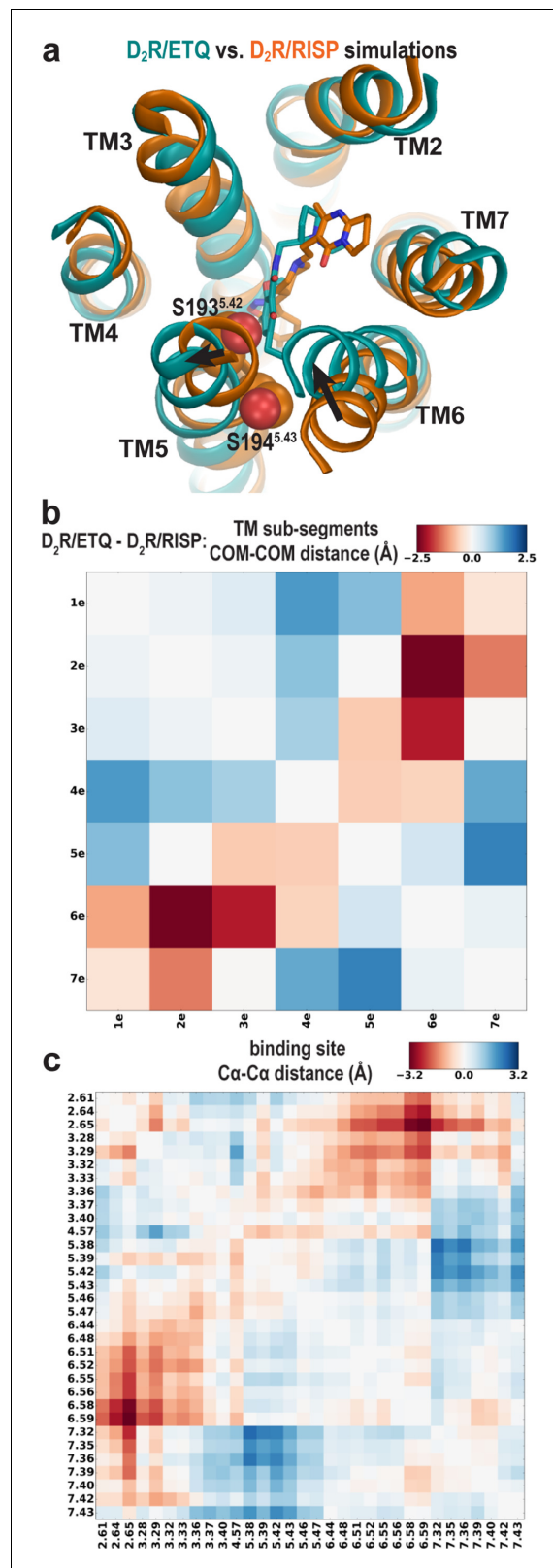


Figure 4. The different conformations in the extracellular vestibules of D_2R and D_3R are likely due to binding of non-selective ligands from different scaffolds. (a) Compared to the comparison of the crystal structures shown in **Figure 1**, superpositioning of representative frames of the D_2R/ETQ and $D_2R/RISP$ simulations shows a similarly trend of the outward and inward movements of TM5 and TM6, respectively, in the presence of the bound ETQ, *Figure 4 continued on next page*

Figure 4 continued

even when the simulations were started from the D₂R conformation stabilized by RISP. Note Ser193^{5.42} and Ser194^{5.43} would clash with the bound eticlopride if there was no conformational adjustment. (b, c) PIA-GPCR analysis (see Materials and methods) comparing the D₂R/ETQ and D₂R/RISP conformations. The analysis of the pairwise-distance differences among the subsegments (b) indicates that TM6e moves inward (smaller distance to TM2e, dark red pixel), while TM5e moves outward (larger distances to TM7e, dark blue pixel) in the D₂R/ETQ simulations. The analysis of pairwise-distance differences among the C α atoms of the ligand-binding residues (c) indicates significant changes near residues Phe189^{5.38}, Ser193^{5.42}, Asn367^{6.58}, and Ile368^{6.59} (darker colored pixels). The online version of this article includes the following figure supplement(s) for figure 4:

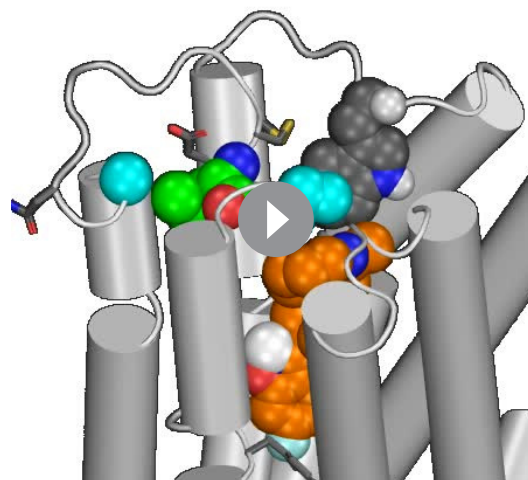
Figure supplement 1. The occupation of the Ile^{3.40} pocket by risperidone is associated with outward movement of the extracellular portion of TM6.

findings further support our inference that differences between the D₂R and D₃R inactive structures are largely due to the different scaffolds of the bound non-selective ligands.

The extracellular loop 2 (EL2) of D₂R/risperidone can spontaneously unwind

In addition to differences in the transmembrane segments surrounding the OBS, there are also substantial differences in the configuration of EL2 in the D₂R and D₃R structures. EL2 between TM4 and TM5 is connected to TM3 via a disulfide bond formed between Cys^{EL2.50} (see Materials and methods and **Figure 5—figure supplement 1** for the indices of EL1 and EL2 residues) and Cys^{3.25}. The conformation of EL2, the sequence of which is not conserved among aminergic GPCRs, is expected to be dynamic. Indeed, in the D₂R/risperidone structure, the sidechains of residues 176^{EL2.40}, 178^{EL2.46}, 179^{EL2.47}, and 180^{EL2.48}, which are distal to the OBS were not solved, likely due to their dynamic nature. Curiously, the portion of EL2 C-terminal to Cys182^{EL2.50} (residues 182^{EL2.50}-186^{EL2.54}), which forms the upper portion of the OBS that is in contact with ligand, is in a helical conformation in the D₂R/risperidone structure.

Strikingly, in our MD simulations of D₂R complexes, we found that this helical region showed a tendency to unwind (**Video 1**). The unwinding of EL2 involves a drastic rearrangement of the sidechain of Ile183^{EL2.51}, which dissociates from a hydrophobic pocket formed by the sidechains of Val111^{3.29}, Leu170^{4.60}, Leu174^{EL2.38}, and Phe189^{5.38}. Specifically, the unwinding process is initiated by the loss of a hydrogen-bond (H-bond) interaction between the sidechain of Asp108^{3.26} and the backbone amine group of Ile183^{EL2.51} formed in the D₂R/risperidone structure (**Figure 5—figure supplement 2b**, step (i)). When this interaction is broken, the orientation of residues 182^{EL2.50}-186^{EL2.54} deviates markedly from that of the crystal structure, losing its helical conformation (see below). Subsequently, the sidechain of Ile183^{EL2.51} rotates outwards and passes a small steric barrier of Gly173^{EL2.37} (**Figure 5—figure**



Video 1. A movie of a 4.2 μ s D₂R/risperidone trajectory collected using the OPLS3e force field shows spontaneous unwinding of EL2. The conformation of EL2 gradually transitions to an extended configuration similar to that in the D₃R structure. See **Figure 5—figure supplement 2** for the pathway of unwinding. Note that the extended conformation of EL2 stabilizes Trp100^{EL1.50}. The C α atom of Gly173^{EL2.37}, the sidechains of Trp100^{EL1.50}, Ile183^{EL2.51}, and Ile184^{EL2.52} and the bound risperidone are shown as spheres. Asp108^{3.26} and the disulfide bond between Cys107^{3.25} and Cys182^{EL2.50} are shown as sticks. The carbon atoms of Gly173^{EL2.37} and Ile184^{EL2.52} are colored in cyan, those of Ile183^{EL2.51} are in green, those of Trp100^{EL1.50}, Cys107^{3.25}, Asp108^{3.26}, Asn175^{EL2.39}, and Cys182^{EL2.50} are in dark gray; those of the bound ligand risperidone are in orange.

<https://elifesciences.org/articles/52189#video1>

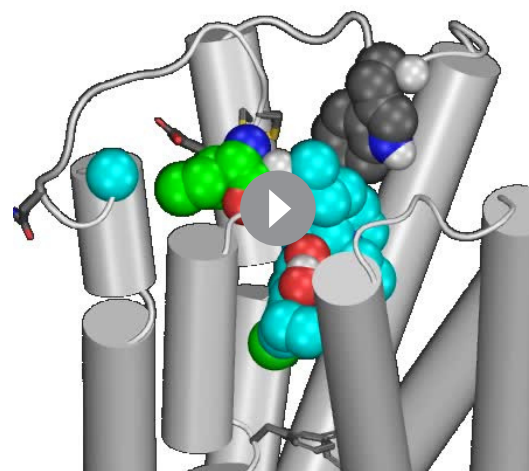
supplement 2b, step (ii), and in some trajectories makes a favorable hydrophobic interaction with the sidechain of Ala177^{EL2.45}. In a few long trajectories, Ile183^{EL2.51} rotates further toward the extracellular vestibule where it can make favorable interactions with hydrophobic or aromatic residues from the N terminus, or the bound risperidone (**Video 1**). Consequently, residues 182^{EL2.50}-186^{EL2.54} are in a fully extended loop conformation while Ile184^{EL2.52} tilts under EL2 (**Figure 5—figure supplement 2b**, step (iii)).

In the D₃R structure, the aligned residue for Asp108^{3.26} of D₂R is conserved as Asp104^{3.26}; its sidechain forms an interaction not with Ile182^{EL2.51} but rather with the sidechain of Asn173^{EL2.39}, which is also conserved in D₂R as Asn175^{EL2.39}. In the D₄R, the aligned two residues (Asp109^{3.26} and Asn175^{EL2.39}) are conserved as well, their sidechains are only 4.3 Å away in the D₄R structure, a distance slightly larger than the 3.2 Å in the D₃R structure. Even though these residues are conserved in D₂R, the interaction in D₃R (and potentially in D₄R), between Asp^{3.26}-Asn^{EL2.39}, is not present in the D₂R structure in which the aligned Asn175^{EL2.39} faces lipid (**Figure 5—figure supplement 2a**). However, in a few of our long D₂R simulations, Asn175^{EL2.39} gradually moves inwards and approaches Asp108^{3.26} (**Figure 5—figure supplement 2b**, step (iv)). At this point, the EL2 conformation of D₂R is highly similar to that of D₃R (**Figure 5—figure supplement 2c**), suggesting that EL2 is dynamic and can exist in both conformations.

We evaluated the tendency of the EL2 helix to unwind in each of the simulated D₂R complexes by measuring the stability of the backbone H-bond between Ile183^{EL2.51} and Asn186^{EL2.54}, a key stabilizing force of the helix (**Figure 5a**). When we plotted the Ile183^{EL2.51}-Asn186^{EL2.54} distance against the Asp108^{3.26}-Ile183^{EL2.51} distance for each D₂R complex (**Figure 5b**), we found that the loss of the Asp108^{3.26}-Ile183^{EL2.51} interaction increases the probability of breaking the Ile183^{EL2.51}-Asn186^{EL2.54} H-bond, that is the unwinding of EL2. Interestingly, in all our simulated D₂R complexes, EL2 has a clear tendency to unwind, regardless of the scaffold of the bound ligand (**Figure 5c,d**, **Videos 1–3**). Note that in the D₃R/eticlopride simulations, the aligned residues Ser182^{EL2.51} and Asn185^{EL2.54} do not form such a H-bond, and EL2 is always in an extended conformation (**Figure 5b–d**). This tendency of EL2 to transition toward the extended conformation is also present in our simulations of D₂R in complex with a partial agonist, aripiprazole, whereas EL2 in the D₃R complexes with partial agonists (R22 and S22) remains in the extended conformation (**Table 1** and **Figure 5—figure supplement 3**). Interestingly, Asp104^{3.26} and Ser182^{EL2.51} can move into interacting range in the D₃R/eticlopride simulations, and the Ser182^{EL2.51}-Asn185^{EL2.54} interaction can sporadically form in the D₃R/R22 simulations – both raise the possibility that the extended conformation of D₃R EL2 may transition to a helical conformation.

Interestingly, in one of our long MD trajectories of the D₂R/risperidone complex, EL2 evolved into a conformation that has a helical N-terminal portion and an extended C-terminal portion (**Video 4** and **Figure 5—figure supplement 4**). This conformation is not observed in either of the D₂R/risperidone and D₃R/eticlopride structures but is similar to that of the 5-HT_{2A}R/risperidone structure, further demonstrating the dynamics of this loop region (**Figure 5—figure supplement 4**).

In marked contrast to the obvious trend toward unwinding of EL2 in all our simulated D₂R complexes, in our recent simulations of MhsT, a transporter protein with a region found by crystallography to alternate between helical and unwound conformations (**Malinauskaite et al., 2014**), we failed to observe any spontaneous unwinding over a similar simulation timescale



Video 2. A movie of a 4.2 μs D₂R/eticlopride trajectory shows the dynamics of Trp100^{EL1.50} when the C-terminal portion of EL2 is in a helical conformation. Note that Trp100^{EL1.50} can be stabilized by interacting with the disulfide bond. The presentation and color scheme are similar to those in **Video 1**, except that the bound carbon atoms of the ligand eticlopride are colored in cyan.

<https://elifesciences.org/articles/52189#video2>

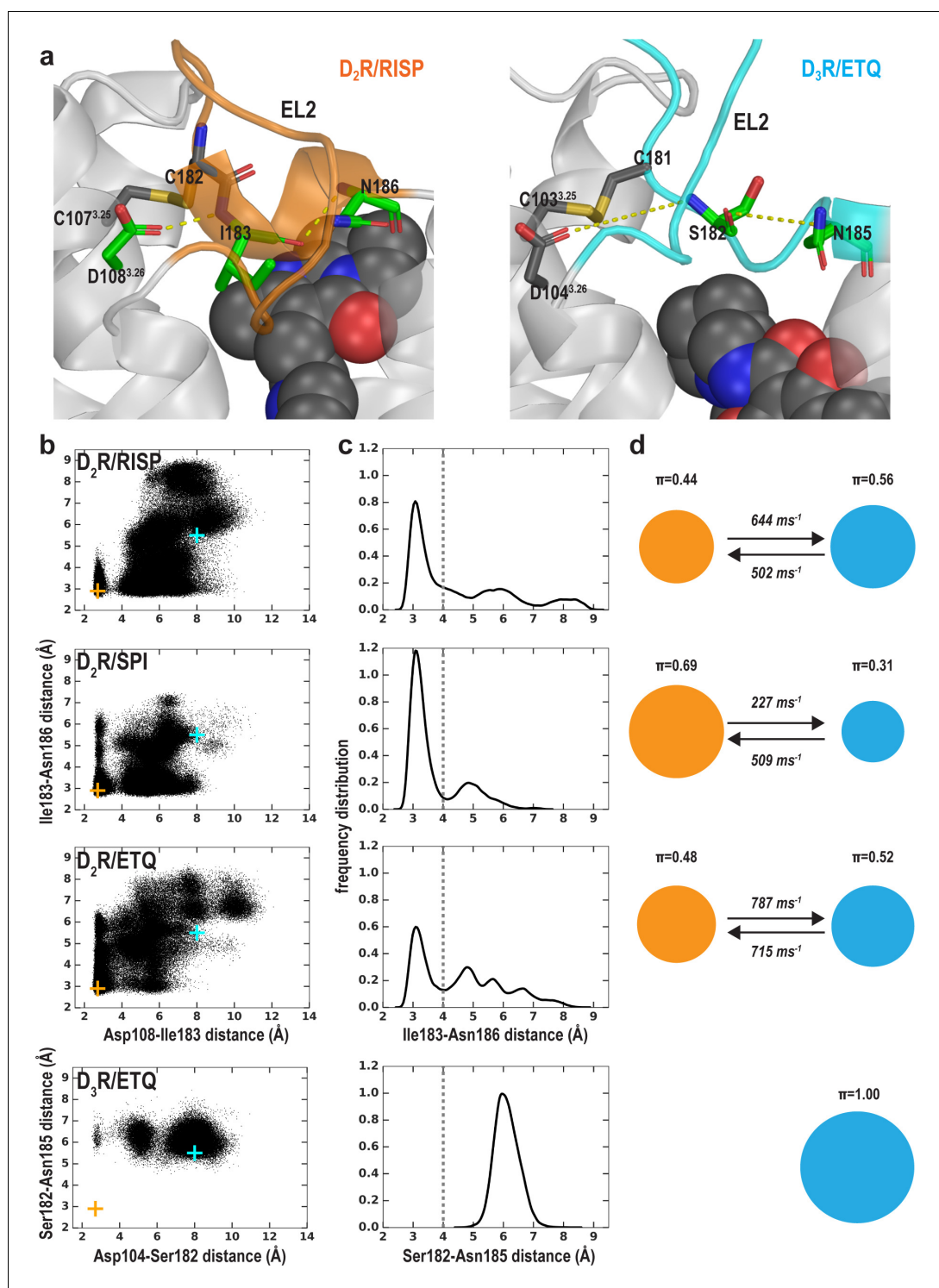


Figure 5. The helical conformation of EL2 in the D₂R/risperidone structure has a tendency to unwind in our simulations, regardless of the bound ligand. (a) The Ile183^{EL2.51}-Asn186^{EL2.54} backbone H-bond and the Ile183^{EL2.51}-Asp108^{3.26} interaction in D₂R and their aligned interactions in D₃R. (b) The scatter plots of the two distances in the indicated D₂R and D₃R complexes. The orange and cyan crosses indicated the distances in the D₂R/risperidone and D₃R/eticlopride structures, respectively. (c) The distributions of the EL2.51-EL2.54 distances in the indicated simulations. These distances were used to evaluate the tendency to unwind using Markov state model (MSM) analysis in d. (d) The MSM analysis of the transition between the helical and extended conformational states of EL2. The area of each disk representing a state is proportional to the equilibrium

Figure 5 continued on next page

Figure 5 continued

probability (π) in each simulated condition. The values from the maximum likelihood Bayesian Markov model for π and transition rates from 500 Bayesian Markov model samples are shown. Thus, EL2 in all the D₂R complexes show significant tendencies to unwind, while that in D₃R/eticlopride remains extended.

The online version of this article includes the following figure supplement(s) for figure 5:

Figure supplement 1. Sequence alignment and residue indices of EL1 and EL2 for the receptors being compared in this study.

Figure supplement 2. The helical region of EL2 of D₂R can spontaneously unwind to an extended conformation similar to that of D₃R.

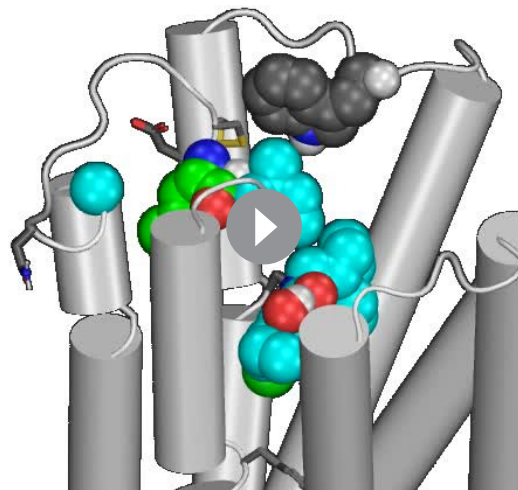
Figure supplement 3. The MSM analysis of Ile183-Asn186 distance in the simulations of the D₂R/aripiprazole, D₃R/S22, and D₃R/R22 complexes (**Table 1**).

Figure supplement 4. The distinct D₂R EL2 conformations revealed by the MD simulations are similar to those of homologous receptors.

Figure supplement 5. The accessibility pattern of EL2 revealed by previous SCAM studies in D₂R is more consistent with an extended EL2 conformation similar to that in the D₃R/eticlopride structure.

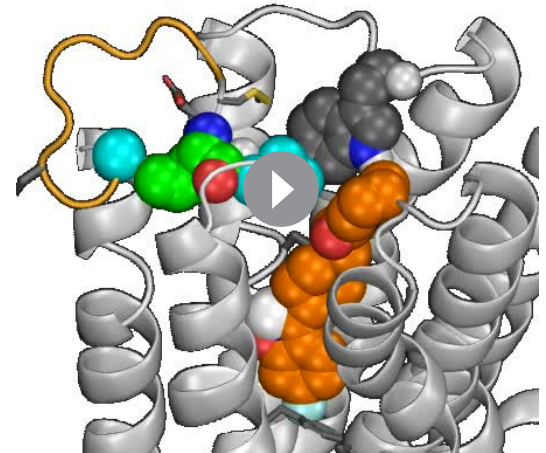
Figure supplement 6. Implied timescales (ITS) for the MSM analysis.

(with the longest simulations being ~5–6 μ s) when the region was started from the helical conformation (**Abramyan et al., 2018; Stolzenberg et al., 2017**). This shows how difficult it can be to capture known dynamics in simulations and suggests that the C-terminal helical conformation of EL2 in D₂R represents a higher energy state than the extended conformation, which allows for observation of the transitions in a simulation timescale not usually adequate to sample folding/unfolding events (**Piana et al., 2011**).



Video 3. A movie of a 3.6 μ s D₂R/eticlopride trajectory collected using the CHARMM36 force field shows another example of unwinding of EL2. Thus, considering the similar unwinding pathway as that in **Video 1** (**Figure 5—figure supplement 2**), the unwinding does not depend on the force field used in the simulations or the identity of the antagonist bound in the OBS. Note the sidechain of Asn175^{EL2.39} rotates inward and approaches Asp108^{3.26} in this trajectory. The presentation and color scheme are the same as those in **Video 2**.

<https://elifesciences.org/articles/52189#video3>



Video 4. A movie of a 4.5 μ s D₂R/risperidone trajectory shows the N-terminal portion of EL2 can transition into a helical conformation when the C-terminal portion is extended. This is a novel EL2 conformation that has not been revealed by the D₂R, D₃R or D₄R structures but similar to those in the 5-HT_{2A}R/risperidone (**Figure 5—figure supplement 4f**), β_1 AR and β_2 AR structures. The presentation and color scheme are the same as those in **Video 1**.

<https://elifesciences.org/articles/52189#video4>

Both the EL2 conformation and ligand scaffold affect the EL1 conformation

We have previously shown that the divergence in both the length and number of charged residues in EL1 among D₂R, D₃R, and D₄R is responsible for the selectivity of more extended ligands (*Michino et al., 2013; Newman et al., 2012*). Another striking difference in the D₂R, D₃R, and D₄R structures is the position of the conserved Trp^{EL1.50} in EL1. Trp100^{EL1.50} is in a much more inward position in the D₂R structure, making a direct contact with the bound risperidone (*Figure 6a*), Trp101^{EL1.50} in D₄R interacts with the bound nemonapride that has an extended structure, whereas Trp96^{EL1.50} in D₃R is not in contact with eticlopride (*Figure 6b*). Thus, we asked whether these distinct positions of Trp^{EL1.50} are due to the divergence in EL1 among these receptors (*Michino et al., 2013*) or due to the multiple inactive conformations that differentially accommodate the binding of non-selective ligands of divergent scaffolds.

When residues 182^{EL2.50}-186^{EL2.54} of EL2 are in a helical conformation, in the D₂R/risperidone simulations, we found that there is more room in the extracellular vestibule and the position of Trp100^{EL1.50} is flexible and can adopt several positions and orientations (*Figure 6c,e,f*). In the D₂R/eticlopride simulations, Trp100^{EL1.50}, which cannot interact with eticlopride, shows more flexibility than that observed in the presence of risperidone and can move to a similar position like that of Trp96^{EL1.50} in the D₃R structure (*Figure 6—figure supplement 1* and *Video 2*). Interestingly, in this position, the conformation of Trp^{EL1.50} can be stabilized by the disulfide bond of EL2 (*Ioerger et al., 1999*) (as shown in *Video 2*) or by interaction with the N terminus, which was truncated in the receptor construct used in the determination of the crystal structure. In the D₂R/spiperone simulations, the phenyl substitution on the triazaspiro[4.5]decane moiety protrudes toward the interface between TM2 and TM3, and contacts Trp100^{EL1.50}, which is flexible as well and can adopt a position that is even further away from the OBS than that of Trp96^{EL1.50} in the D₃R structure (*Figure 6—figure supplement 1*).

In contrast, when EL2 is in an extended conformation like that in D₃R, it restricts the flexibility of Trp100^{EL1.50} (*Video 3*). This trend is consistent with the D₃R/eticlopride simulations in which we do not observe any significant rearrangement of Trp96^{EL1.50} (*Figure 6d,e,f*).

Thus, we infer that the distinct conformation of Trp100^{EL1.50} in the D₂R structure is a combined effect of the helical EL2 conformation and the favored interaction that Trp100^{EL1.50} can form with the bound risperidone in the crystal structure, the latter of which however, has a limited influence on the binding affinity of risperidone (*Wang et al., 2018*), consistent with the unstable interaction between risperidone and Trp100^{EL1.50} in our simulations (*Figure 6, Video 2*). Indeed, in the fully extended EL2 conformation in which Ile183^{EL2.51} rotates to face the extracellular vestibule, Ile183^{EL2.51} makes a direct contact with the bound risperidone, whereas Trp100^{EL1.50} loses its interaction with the ligand entirely (*Video 1*). Nevertheless, risperidone retains all other contacts in the OBS. In the recently reported 5-HT_{2A}R/risperidone structure (PDB: 6A93) *Kimura et al. (2019)*, risperidone has a very similar pose in the OBS as that in the D₂R structure, occupying the Ile^{3.40} sub-pocket as well. However, on the extracellular side of the OBS, EL2 in the 5-HT_{2A}R/risperidone complex is in an extended conformation and the EL2 residue Leu228^{EL2.51} contacting risperidone aligns to Ile183^{EL2.51} of D₂R, whereas the conserved Trp141^{EL1.50} does not interact with risperidone in the 5-HT_{2A}R. It is tempting to speculate that the EL2 and EL1 dynamics we observe in the D₂R/risperidone simulations represents a more comprehensive picture, as the divergent interactions shown in the extracellular loops of the 5-HT_{2A}R/risperidone and D₂R/risperidone structures may not result from differences in the protein sequences of this dynamic region between these two receptors but rather two different static snapshots due to differences in the crystallographic conditions (Note risperidone has similarly high affinities for both D₂R and 5HT_{2A}R; *Kimura et al., 2019; Wang et al., 2018*).

Thus, the plasticity of the OBS and the dynamics of the extracellular loops appear to be two relatively separated modules in ligand recognition. To the extent of our simulations, we did not detect strong ligand-dependent bias in the EL2 dynamics as we did for the OBS. However, when EL2 is helical, the EL1 dynamics are sensitive to the bound ligand (compare *Figure 6* and *Figure 6—figure supplement 1*); when EL2 is extended, it restricts EL1 dynamics (*Figure 6*).

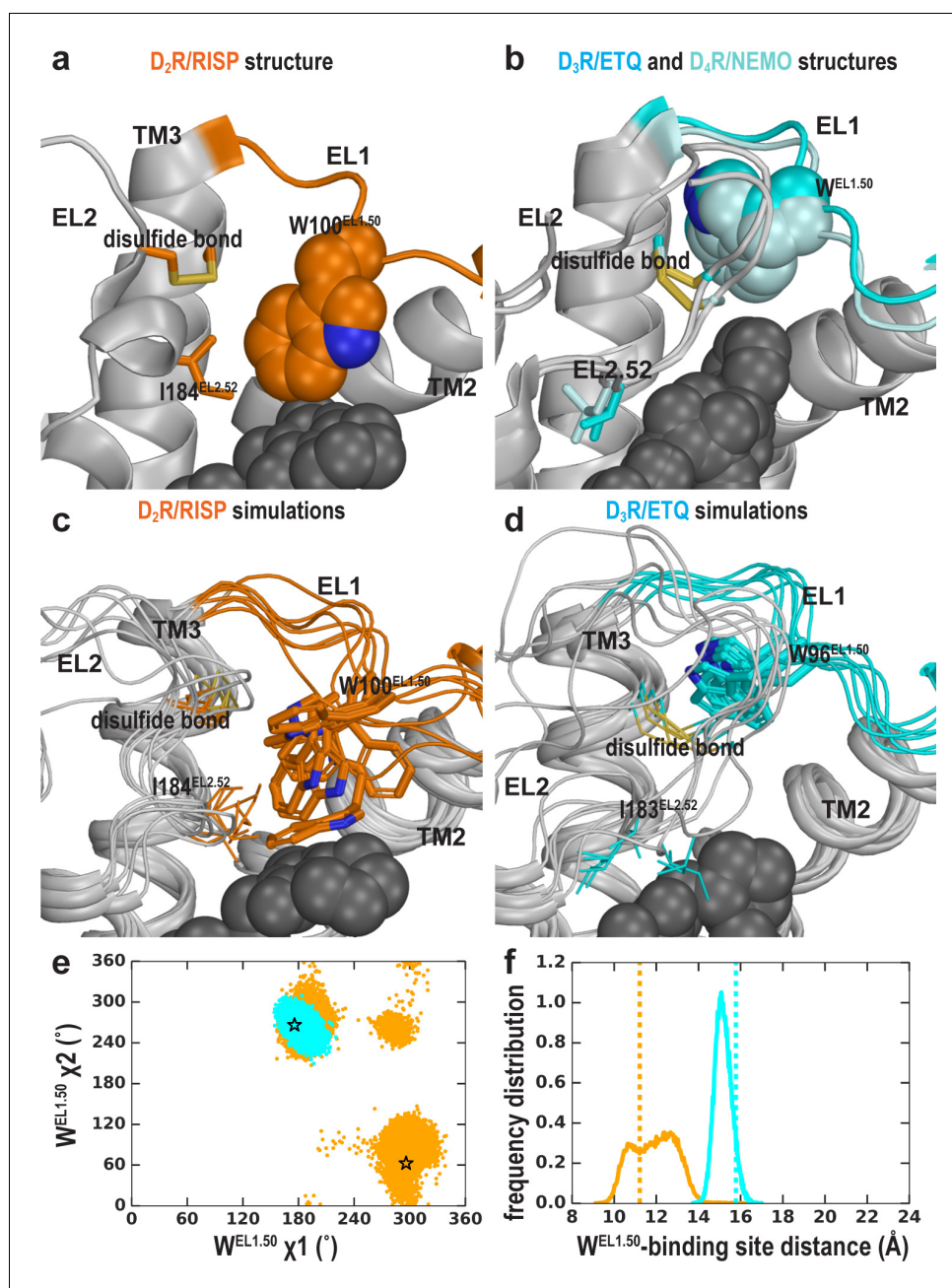


Figure 6. The EL2 conformation affects the EL1 conformation. Divergent EL1-EL2 interfaces among the D_2R (a), D_3R , and D_4R (b) structures. In the D_2R structure, the Trp100^{EL1.50} in EL1 forms a weak interaction with Ile184^{EL2.52}, while the aligned Trp96^{EL1.50} of D_3R and Trp101^{EL1.50} in D_4R are stabilized by their interactions with the disulfide bond – their passages toward the position of Trp100^{EL1.50} in D_2R are blocked by the extended EL2. In our simulations, Trp100^{EL1.50} in D_2R shows significant flexibility and can adopt multiple positions and orientations in D_2R /risperidone (c), while Trp96^{EL1.50} in D_3R is highly stable in D_3R /eticlopride (d). (e) The χ_1 and χ_2 dihedral angles of Trp100^{EL1.50} in the subset of the D_2R /risperidone simulations in which EL2 is still in a helical conformation (orange), are more widely distributed than those of Trp96^{EL1.50} in the D_3R /eticlopride simulations in which EL2 remains in extended conformations (cyan). These dihedral angle values in the D_2R and D_3R structures are indicated with the orange and cyan stars, respectively. (f), For the same two sets of simulations in e, the distance between the center of mass (COM) of the sidechain heavy atoms of Trp100 in D_2R and the COM of the C α atoms of the ligand-binding site residues (excluding Trp100, see Materials and methods for the list of the residues) has wider distributions than the corresponding distance between Trp96^{EL1.50} in D_3R and its ligand binding site. These distances in the D_2R and D_3R structures are indicated with the orange and cyan dotted lines, respectively.

Figure 6 continued on next page

Figure 6 continued

The online version of this article includes the following figure supplement(s) for figure 6:

Figure supplement 1. EL1 is dynamic in the D₂R/eticlopride and D₂R/spiperone simulations when EL2 is helical.**Figure supplement 2.** Trp^{EL1.50} is closely associated with Leu^{2.64} regardless of the EL2 conformation.

The Ile184^{EL2.52}-Trp100^{EL1.50} interaction is not critical for risperidone binding

To further investigate the dynamics and coordination of EL2 and EL1 loops, we mutated Leu94^{2.64}, Trp100^{EL1.50}, and Ile184^{EL2.52}, and evaluated the effects of the L94A, W100A, and I184A, mutations on the binding affinities of eticlopride, risperidone, and spiperone. As shown in **Figure 6—figure supplement 2**, Leu94^{2.64} and Trp100^{EL1.50} are closely associated in both the D₂R and D₃R structures, while Ile184^{EL2.52} interacts with Trp100^{EL1.50} only in the D₂R structure. In our time-resolved energy transfer (Tr-FRET) binding experiments, using a fluorescently labeled spiperone derivative (spiperone-d2) as a tracer ligand, we found that both L94A and W100A significantly reduced the affinities of all tested antagonists, whereas I184A only reduced the affinity of eticlopride while it improved that of risperidone (**Table 3**). Thus, the effects of the L94A and W100A mutations have similar trends, which appear independent of the effect of I184A. Indeed, for Trp100 to switch between the positions in the D₂R and D₃R structures, it must pass the steric hinderance of the sidechain of Leu94; thus, some effects of the L94A mutation may reflect its perturbation of the positioning of Trp100, and vice versa.

These findings support our conclusions that the close interaction between Ile184^{EL2.52} and Trp100^{EL1.50} revealed by the D₂R/risperidone crystal structure is not necessary for the stabilization of the risperidone pose. Indeed, in our simulations, EL2 has significant intrinsic dynamics and transitions from the helical to unwound conformation independent of the bound ligands (see above). When it is in an extended conformation, Ile184 is dissociated from Trp100.

The clustering of the binding site conformations

Virtual screening has been widely used as an initial step in drug discovery for novel ligand scaffolds. To this end, we found that D₂R can significantly change its binding site shape to accommodate antagonists bearing different scaffolds, while EL2 is intrinsically dynamic. Thus, it is necessary to comprehensively consider the binding site conformations in virtual screening campaigns against D₂R, because limiting the screening to only a single conformation will miss relevant ligands. Indeed,

Table 3. The effect of mutations on the binding affinities of selected D₂R ligands as determined in Tr-FRET-binding experiments. The affinities of the fluorescently labeled spiperone derivative (Spiperone-d2) or unlabeled antagonists were determined in saturation experiments at WT or mutant SNAP-tagged D₂Rs stably expressed in FlpIn CHO cells. Binding affinity values for risperidone and eticlopride were obtained in competition binding experiments. Means of n independent experiments are shown with 95% confidence intervals (CIs).

SNAP-D ₂ R	Spiperone-d2 saturation binding			Spiperone-d2 competition binding								
	pK _d (K _d , nM) (95% CI)	N	Mut/WT	Eticlopride pK _i (K _i , nM) (95% CI)		Risperidone pK _i (K _i , nM) (95% CI)		Spiperone pK _i (K _i , nM) (95% CI)				
WT	8.54 (2.88) (8.32–8.77)	9	1.0	10.06 (0.09) (9.90–10.21)	8	1.0	8.47 (3.34) (8.15–8.80)	7	1.0	9.96 (0.11) (9.76–10.18)	8	1.0
L94A	7.71 (19.5) (7.41–8.00)*	5	6.8	9.08 (0.83) (8.91–9.23)*	4	9.2	8.02 (9.54) (7.86–8.17)*	5	2.9	8.36 (4.37) (8.21–8.50)*	5	39.7
W100A	7.39 (40.7) (7.21–7.56)*	9	14.1	8.06 (8.71) (7.78–8.32)*	4	96.8	7.60 (25.1) (7.41–7.79)*	7	7.5	8.39 (4.07) (8.19–8.59)*	7	37.0
I184A	8.79 (1.62) (8.58–9.00)	5	0.6	9.34 (0.45) (8.94–9.75)*	4	5	9.33 (0.47) (9.18–9.48)*	5	0.1	9.78 (0.17) (9.51–10.05)	5	1.6

*=significantly different from WT value, p<0.05, one-way ANOVA with Dunnett's post-hoc test.

the strategy of ensemble docking, in which each ligand is docked to a set of receptor conformers, has been adapted in recent virtual screening efforts (Amaro *et al.*, 2018).

To characterize the OBS conformational ensemble sampled by D₂R in complex with ligands bearing different scaffolds in the context of EL2 dynamics, we clustered the OBS conformations in our representative D₂R/eticlopride and D₂R/risperidone MD trajectories in which EL2 transitioned from helical to unwound conformations (see Materials and methods). As expected, the OBS conformations in these two complexes are significantly different and can be easily separated into distinct clusters. For the clustering results shown in **Table 4**, the average pairwise RMSDs of the OBS residues (apRMSDs, see Materials and methods) between the D₂R/eticlopride and D₂R/risperidone clusters are >1.1 Å, which are similar to that between the D₂R and D₃R structures (1.2 Å), while the apRMSDs within each cluster is smaller than those between any two clusters (**Figure 7**). Interestingly, at this level of clustering, when the two clusters for each complex are ~0.8–0.9 Å apRMSD away from each other, the extended and helical conformations of EL2 are always mixed in a cluster (**Table 4**). This observation suggests that the helical versus extended EL2 conformations are not closely associated with the OBS conformations.

Thus, while the centroid frames from each cluster can form an ensemble for future virtual screening for the primary scaffold occupying the OBS, in order to discover novel extended ligands that protrude out of the OBS to interact with EL2 and EL1 residues (Michino *et al.*, 2015a), additional frames that cover both helical and extended EL2 conformations from each cluster will have to be used to screen for the optimal extensions of the primary scaffold.

Discussion

Our results highlight unappreciated conformational complexity of the inactive state of GPCRs and suggest that the risperidone bound D₂R structure represents only one of a number of possible inactive conformations of D₂R. Critically, this conformation is incompatible with the binding of other high-affinity D₂R ligands such as eticlopride. While distinct conformational states responsible for functional selectivity have garnered great attention, the potential existence of divergent inactive conformations is of critical importance as well. By combining *in silico* and *in vitro* findings, we propose that occupation of the Ile^{3.40} sub-pocket by antagonists confers a distinct D₂R conformation that is associated with both a greater degree of inverse agonism and Na⁺ insensitivity in binding, such that Na⁺ sensitivity is negatively related with the extent of inverse agonism for the tested ligands. However, other structural elements may also contribute to the extent of inverse agonism (Zhang *et al.*, 2014). Regardless, the distinct inactive conformations stabilized by antagonists with different scaffolds may reflect different degrees of inactivation.

In addition to advancing our mechanistic understanding of receptor function, our findings have implications for high-throughput virtual screening campaigns, as important hits would be missed by focusing on a single inactive state captured in a crystal structure that is stabilized by an antagonist bearing a specific scaffold. Moreover, rational lead optimization requires rigorous physical

Table 4. Clustering results of the OBS conformations sampled in the D₂R/eticlopride and D₂R/risperidone simulations.

The compositions in each cluster are shown as percentages of the frames randomly extracted for each complex (see Materials and methods), when sorted by either receptor/ligand complex or EL2 conformation.

Cluster ID	Percentage (%)							
	Complex				EL2 conformation			
	D ₂ R/eticlopride		D ₂ R/risperidone		Extended		Helical	
	Mean	Sd	Mean	Sd	Mean	Sd	Mean	Sd
1	38.4	0.7	0.0	0.0	4.9	0.4	33.5	0.5
2	61.6	0.7	0.0	0.0	45.1	0.4	16.5	0.6
3	0.0	0.0	43.7	1.0	2.5	0.4	41.3	0.8
4	0.0	0.0	56.3	1.0	47.5	0.4	8.7	0.8

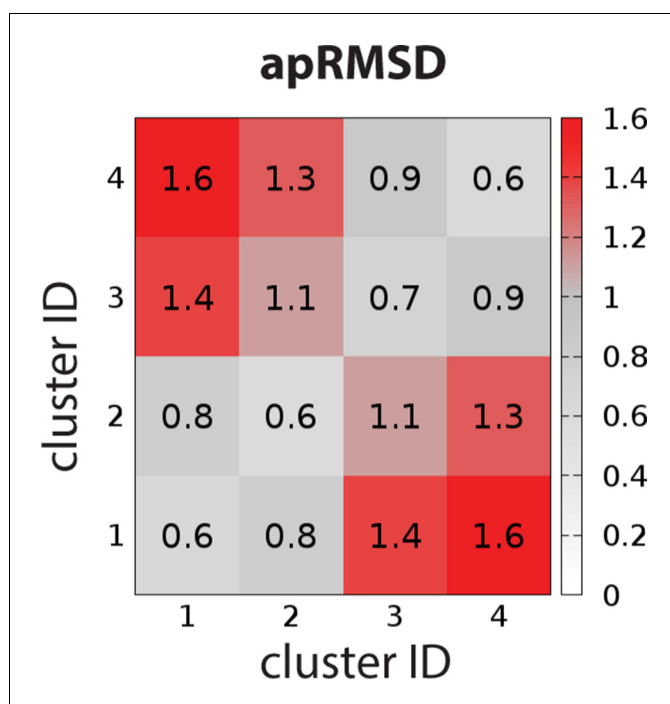


Figure 7. The average pairwise RMSDs of the clusters of the OBS conformations. The clustering level was chosen to be 4, so that the average pairwise RMSDs (apRMSDs) between the D₂R/eticlopride clusters (1 and 2, see **Table 4** for the composition of each cluster) and D₂R/risperidone clusters (3 and 4) are similar to that between D₂R and D₃R structures (1.2 Å), while all the apRMSDs within a cluster are smaller than those between any given two clusters.

description of molecular recognition (*Beuming and Shi, 2017*), which depends on adequate understanding of the conformational boundary and flexibility of the targeted state. We have shown previously that both dopamine receptor subtype selectivity and modulation of agonist efficacy can be achieved through the design of ligands that extend from the OBS into an extracellular secondary binding pocket (SBP) (*Michino et al., 2015a; Newman et al., 2012*). We now show that one might consider the occupation of the Ile^{3.40} sub-pocket in the process of decorating an D₂R antagonist scaffold to attain a desired level of inverse agonism. Our findings also reveal allosteric communication between the Ile^{3.40} sub-pocket and the Na⁺-binding site. Thus, Na⁺ sensitivity in antagonist binding may provide useful mechanistic insights as part of such efforts.

The mutation of Trp100^{EL1.50} in D₂R to alanine, leucine or phenylalanine cause substantial increases in both the association and dissociation rate of risperidone (*Wang et al., 2018*). Curiously, both the dissociation and association rates of D₂R antagonists used as antipsychotics have been proposed to determine their propensity to cause extrapyramidal side-effects and hyperprolactinaemia (*Seeman, 2014; Sykes et al., 2017*). Our results indicate that both the EL2 conformation and antagonist scaffolds may influence the dynamics of Trp100^{EL1.50}, which in turn controls ligand access and egress to and from the OBS. Thus, understanding the relationship between the distinct inactive D₂R conformations stabilized by different antagonist scaffolds and these kinetic parameters will likely be important to facilitate the design of D₂R antagonists with an optimal kinetic profile that minimizes the risk of side effects.

Previously, using the substituted-cysteine accessibility method (SCAM) in D₂R (*Javitch et al., 2000; Shi and Javitch, 2004*), we found that G173^{EL2.37C}, N175^{EL2.39C}, and I184^{EL2.52C} were accessible to charged MTS reagents and that this accessibility could be blocked by the bound Na⁺-sensitive antagonist sulpiride, consistent with their water accessibility and involvement in ligand binding and not with a static orientation facing lipid, whereas A177^{EL2.45C} and I183^{EL2.51C} were accessible but not protected by sulpiride. Curiously, in the D₂R/risperidone structure, Ile184^{EL2.52} is only marginally in contact with the ligand, Ile183^{EL2.51} blocks the accessibility of Gly173^{EL2.37} to the OBS and

is itself buried in a hydrophobic pocket, whereas Asn175^{EL2.39} faces lipid, where it would be much less reactive. In the D₃R/eticlopride structure, Ile183^{EL2.52} is in close contact with the bound ligand, Ser182^{EL2.51} faces the extracellular vestibule, whereas the sidechain of Asn173^{EL2.39} is oriented toward the OBS (**Figure 5—figure supplement 5**). Thus, our analysis shows that the accessibility pattern of EL2 revealed by previous SCAM studies in D₂R are more consistent with the extended EL2 conformation revealed by the D₃R/eticlopride structure but not with the D₂R/risperidone structure. Indeed, we observed spontaneous transitions of EL2 from a helical to extended conformation in our D₂R simulations, which suggests that EL2 of D₂R exists in an ensemble of structured and unwound conformations, with substantial occupation of the configuration found in the D₃R structure. Such dynamics of EL2 suggest that the drastically different conformations between the D₂R and D₃R structures near EL2 are not related to the divergence of the receptors. Thus, the D₂R EL2 appears to have quite dramatic dynamics that are not captured by the crystal structure.

Taken together, our findings reveal that both the plasticity of the transmembrane domain in accommodating different scaffolds and the dynamics of EL2 and EL1 are important considerations in RDD targeting the inactive conformation of D₂R.

Materials and methods

Key resources table

Reagent type (species) or resource	Designation	Source or reference	Identifiers	Additional information
Cell line (<i>Cricetulus griseus</i>)	FlpIn CHO	Invitrogen	Cat# R75807	
Transfected construct (human)	SNAP-D ₂ S _R	Cisbio	Cat# pSNAPD2	
Transfected construct (human)	D ₂ R G α_{sA} -RLuc8 G β 1 G γ 2-Venus	<i>Michino et al., 2017</i>	N/A	
Commercial assay or kit	Spiperone-d2 SNAP-Lumi4-Tb 5x SNAP/CLIP labeling medium	Cisbio	Cat# L0002RED Cat# SSNPTBX Cat# LABMED	
Chemical compound, drug	Na bisulfite Glucose (+)-Butaclamol Risperidone Haloperidol	Sigma Aldrich	Cat# 243973 Cat# D9434 Cat# D033 Cat# R3030 Cat# H1512	
Chemical compound, drug	Spiperone	Cayman chemicals	Cat# 19769	
Chemical compound, drug	Eticlopride HCl Raclopride (-)-Sulpiride Quinpirole	Tocris Bioscience	Cat# 1847 Cat# 1810 Cat# 0895 Cat# 1061	
Chemical compound, drug	[³ H]spiperone	Perkin Elmer	Cat# NET1187250UC	
Chemical compound, drug	Polyethylenimine	Polysciences	Cat# 23966	
Chemical compound, drug	Coelenterazine-h	NanoLight Technology	Cat# 301–5	
Software, algorithm	Prism	GraphPad	v7.0 and v8.2.1	

Residue indices in EL1 and EL2

Based on a systematic analysis of aminergic receptors, we found a Trp in the middle of EL1 and the disulfide-bonded Cys in the middle of EL2 are the most conserved residues in each segment, and defined their residue indices as EL1.50 and EL2.50, respectively (*Michino et al., 2015a*). In this study, for the convenience of comparisons among D₂R, D₃R, and D₄R, and 5-HT_{2A}R, based on the

alignments of EL1 And EL2 shown in **Figure 5—figure supplement 1**, we index the EL1 and EL2 residues of each receptor in the same way as the Ballesteros-Weinstein numbering, for example the residues before and after the EL2.50 are EL2.49 and EL2.51, respectively. Note the indices for the shorter sequences are not necessarily be consecutive, given the gaps in the alignment.

Molecular modeling and docking

The D₂R models in this study are based on the corrected crystal structure of D₂R bound to risperidone (PDB: 6CM4) (Wang et al., 2018). We omitted T4 Lysozyme fused into intracellular loop 3. Three thermostabilizing mutations (Ile122^{3.40}A, L375^{6.37}A, and L379^{6.41}A) were reverted to their WT residues. The missing N terminus in the crystal structure was built de novo using Rosetta (Bradley et al., 2005), and then integrated with the rest of the D₂R model using Modeller (John and Sali, 2003). Using Modeller, we also extended two helical turns at the TM5 C terminus and three residues at the TM6 N terminus of the structure and connected these two ends with a 9 Gly loop, similar to our experimentally validated treatment of D₃R models (Michino et al., 2017). The position of the Na⁺ bound in the canonical Na⁺-binding site near the negatively charged Asp^{2.50} was acquired by superimposing the Na⁺-bound structure of adenosine A_{2A} receptor (Liu et al., 2012) to our D₂R models.

The binding poses of risperidone and eticlopride were taken according to their poses in the D₂R (Wang et al., 2018) and D₃R (Chien et al., 2010) structures, respectively. Docking of spiperone in our D₂R model was performed using the induced-fit docking (IFD) protocol (Sherman et al., 2006) in the Schrodinger software (release 2017–2; Schrodinger, LLC: New York NY). Based on our hypothesis regarding the role of the Ile^{3.40} sub-pocket in the Na⁺ sensitivity (see text), from the resulting poses of IFD, we choose the spiperone pose with the F-substitution on the butyrophenone ring occupying the Ile^{3.40} sub-pocket. Note that in risperidone and spiperone the F-substitutions have similar distances to the protonated N atoms that interact with Asp^{3.32} (measured by the number of carbon atoms between them, **Figure 1—figure supplement 1**).

Molecular dynamics (MD) simulations

MD simulations of the D₂R and D₃R complexes were performed in the explicit water and 1-palmitoyl-2-oleoylphosphatidylcholine (POPC) lipid bilayer environment using Desmond MD System (version 4.5; D. E. Shaw Research, New York, NY) with either the OPLS3e force field (Roos et al., 2019) or the CHARMM36 force field (Best et al., 2012; Klauda et al., 2010; MacKerell et al., 1998; MacKerell et al., 2004) and TIP3P water model. For CHARMM36 runs, the eticlopride parameters were obtained through the GAAMP server (Huang and Roux, 2013), with the initial force field based on CGenFF assigned by ParamChem (Vanommeslaeghe et al., 2010). The system charges were neutralized, and 150 mM NaCl was added. Each system was first minimized and then equilibrated with restraints on the ligand heavy atoms and protein backbone atoms, followed by production runs in an isothermal–isobaric (NPT) ensemble at 310 K and one atm with all atoms unrestrained, as described previously (Michino et al., 2017; Michino et al., 2015b). We used Langevin constant pressure and temperature dynamical system (Feller et al., 1995) to maintain the pressure and the temperature, on an anisotropic flexible periodic cell with a constant-ratio constraint applied on the lipid bilayer in the X-Y plane. For each condition, we collected multiple trajectories, the aggregated simulation length is ~392 μs (**Table 1**).

While the majority of our D₂R simulations in this study used the OPLS3e force field, to compare with the D₃R simulations using CHARMM36 that have been continued from the previously reported shorter trajectories (Michino et al., 2017; Michino et al., 2015b), we carried out the D₂R/eticlopride simulations using both the OPLS3e and CHARMM36 force fields (see **Table 1**). We did not observe significant differences and pooled their results together for the analysis.

Conformational analysis

Distances and dihedral angles of MD simulation results were calculated with MDTraj (version 1.8.2) (McGibbon et al., 2015) in combination with *in-house* Python scripts.

To characterize the structural changes in the receptor upon ligand binding, we quantified differences of structural elements between the D₂R/eticlopride and D₂R/risperidone conditions (using last 600 ns from a representative trajectory for each condition), by applying the previously described

pairwise interaction analyzer for GPCR (PIA-GPCR) (*Michino et al., 2017*). The subsegments on the extracellular side of D₂R were defined as following: TM1e (the extracellular subsegment (e) of TM1, residues 31–38), TM2e (residues 92–96), TM3e (residues 104–113), TM4e (residues 166–172), TM5e (residues 187–195), TM6e (residues 364–369), and TM7e (residues 376–382).

For the PIA-GPCR analysis in **Figure 4** and the distance analysis in **Figure 6**, we used the set of ligand-binding residues previously identified by our systematic analysis of GPCR structures. Specifically, for D₂R, they are residues 91, 94, 95, 100, 110, 111, 114, 115, 118, 119, 122, 167, 184, 189, 190, 193, 194, 197, 198, 353, 357, 360, 361, 364, 365, 367, 368, 376, 379, 380, 383, 384, 386, and 387; for D₃R, they are residues 86, 89, 90, 96, 106, 107, 110, 111, 114, 115, 118, 165, 183, 188, 189, 192, 193, 196, 197, 338, 342, 345, 346, 349, 350, 352, 353, 362, 365, 366, 369, 370, 372, and 373.

For the clustering of the OBS conformations, we used representative D₂R/eticlopride and D₂R/risperidone MD trajectories in which EL2 transitioned from the helical to unwound conformations. For each complex, using the Ile183-Asn186 distance as a criterion to differentiate the EL2 conformation (**Figure 5**), 1000 MD frames with helical EL2 conformations and another 1000 frames with extended EL2 conformations were randomly selected. For these 4000 frames, the pairwise RMSD of the backbone heavy atoms of the OBS residues defined in *Michino et al. (2015a)*, except for Ile184^{EL2.52}, were calculated. The resulting 4000 × 4000 matrix was used to cluster these frames using the k-mean algorithm implemented in R. We chose nstart to be 20 to assure the convergence of cluster centroids and boundaries. We chose the clustering level to be 4, so that the average pairwise RMSDs (apRMSDs) between the D₂R/eticlopride and D₂R/risperidone clusters are similar to that between D₂R and D₃R structures (1.2 Å), while all the apRMSDs within a cluster are smaller than those between any given two clusters. The same frame selection and clustering procedure was repeated to 20 times. The averages of these 20 runs for the compositions of each cluster were reported in **Table 4**.

Markov State Model (MSM) analysis

The MSM analysis was performed using the pyEMMA program (version 2.5.5) (*Scherer et al., 2015*). To characterize the dynamics of EL2 of D₂R, specifically the transitions between helical and extended conformations of its C-terminal portion, we focused on a key hydrogen bond formed in the helical conformation between the backbone carbonyl group of Ile183 and the backbone amine group of Asn186. Thus, for each of the simulated conditions, the distance of Ile183-Asn186 (Ser182-Asn185 in D₃R) was used as an input feature for the MSM analysis. We discretized this feature into two clusters – distances below and above 4 Å (i.e. EL2 forming a helical conformation and unwinding). Implied relaxation timescale (ITS) (*Swope et al., 2004*) for the transition between these clusters was obtained as a function of various lag times. Convergences of ITS for the MSMs for all conditions was achieved at a lag time of 300 ns (**Figure 5—figure supplement 6**), which we further used to estimate Bayesian Markov models with 500 transition matrix samples (*Trendelkamp-Schroer and Noé, 2013*). The maximum likelihood transition matrix was used to calculate the transition and equilibrium probabilities (π) shown in **Figure 5** and **Figure 5—figure supplement 3**.

Cell culture and cell line generation

Site-directed mutagenesis was performed using the Quickchange method using pEF5/DEST/FRT plasmid encoding FLAG-SNAP-D₂₅R as the DNA template. The mutagenesis was confirmed, and the full coding region was checked using Sanger sequencing at the DNA Sequencing Laboratory (University of Nottingham). Stable cell lines were generated using the Flp-In recombination system (Invitrogen).

[³H]spiperone binding assay

FlpIn CHO cells (Invitrogen) stably expressing WT or mutant SNAP-D₂₅s cells were cultured before the preparation of cell membrane as described before (*Klein Herenbrink et al., 2019*). All stable cell lines were confirmed to be mycoplasma free. For saturating binding assays cell membranes (Mutant or WT SNAP-D₂₅-FlpIn CHO, 2.5 μg) were incubated with varying concentrations of [³H]spiperone and 10 μM haloperidol as a non-specific control, in binding buffer (20 mM HEPES, 100 mM NaCl, 6 mM MgCl₂, 1 mM EGTA, and 1 mM EDTA, pH 7.4) to a final volume of 200 μL and were incubated at 37°C for 3 hr. For competition binding assays, cell membranes (SNAP-D₂₅-FlpIn CHO,

2.5 μg) were incubated with varying concentrations of test compound in binding buffer containing 0.2 nM of [^3H]spiperone to a final volume of 200 μL and were incubated at 37°C for 3 hr. Binding was terminated by fast-flow filtration using a Uniplate 96-well harvester (PerkinElmer) followed by five washes with ice-cold 0.9% NaCl. Bound radioactivity was measured in a MicroBeta2 LumiJET MicroBeta counter (PerkinElmer). Data were collected from at least three separate experiments performed in triplicate and analysed using non-linear regression (Prism 7, Graphpad software). For radioligand saturation binding data, the following equation was globally fitted to nonspecific and total binding data:

$$Y = \frac{B_{\max}[A]}{[A] + K_A} + NS[A] \quad (1)$$

where Y is radioligand binding, B_{\max} is the total receptor density, [A] is the free radioligand concentration, K_A is the equilibrium dissociation constant of the radioligand, and NS is the fraction of non-specific radioligand binding. The B_{\max} of the SNAP-tagged D2SRs were as follows; WT = 7.95 ± 1.63 pmol.mg $^{-1}$, 6.39 ± 1.04 pmol.mg $^{-1}$, 4.37 ± 0.92 pmol.mg $^{-1}$, 2.61 ± 0.50 pmol.mg $^{-1}$.

For competition binding assays, the concentration of ligand that inhibited half of the [^3H]spiperone binding (IC_{50}) was determined by fitting the data to the following equation:

$$Y = \frac{\text{Bottom} + (\text{Top} - \text{Bottom})}{1 + 10^{(X - \text{LogIC}_{50})n_H}} \quad (2)$$

where Y denotes the percentage specific binding, Top and Bottom denote the maximal and minimal asymptotes, respectively, IC_{50} denotes the X-value when the response is midway between Bottom and Top, and n_H denotes the Hill slope factor. IC_{50} values obtained from the inhibition curves were converted to K_i values using the Cheng and Prusoff equation. No statistical methods were used to predetermine sample size.

Bioluminescence resonance energy transfer (BRET) assay

The Go-protein activation assay uses a set of BRET-based constructs previously described (*Michino et al., 2017*). Briefly, HEK293T cells were transiently co-transfected with pcDNA3.1 vectors encoding (i) D₂R, (ii) $G\alpha_{oA}$ fused to Renilla luciferase 8 (RLuc8; provided by Dr. S. Gambhir, Stanford University, Stanford, CA) at residue 91, (iii) untagged G β 1, and (iv) G γ 2 fused to mVenus. Transfections were performed using polyethyleneimine (PEI) at a ratio of 2:1 (PEI:total DNA; weight:weight), and cell culture was maintained as described previously (*Bonifazi et al., 2019*). After ~48 hr of transfection, cells were washed with PBS and resuspended in PBS + 0.1% glucose + 200 μM Na Bisulfite buffer. Approximately 200,000 cells were then distributed in each well of the 96-well plates (White Lumitrac 200, Greiner bio-one). 5 μM Coelenterazine H, a luciferase substrate for BRET, was then added followed by addition of vehicle and test compounds using an automated stamp transfer protocol (Nimbus, Hamilton Robotics) from an aliquoted 96-well compound plate. Following ligands were used – quinpirole, eticlopride, raclopride, and (-)-sulpiride (Tocris Bioscience), (+)-butaclamol, dopamine, and risperidone (Sigma Aldrich), and Spiperone (Cayman chemicals). mVenus emission (530 nm) over RLuc 8 emission (485 nm) were then measured after 30 min of ligand incubation at 37°C using a PHERAstar FSX plate reader (BMG Labtech). BRET ratio was then determined by calculating the ratio of mVenus emission over RLuc eight emission.

Data were collected from at least nine independent experiments and analyzed using Prism 7 (GraphPad Software). Drug-induced BRET, defined by BRET ratio difference in the presence and absence of compounds, was calculated. Concentration response curves (CRCs) were generated using a non-linear sigmoidal dose-response analyses using Prism 7 (GraphPad Software). CRCs are presented as mean drug-induced BRET \pm SEM. E_{\max} bar graphs are plotted as the percentage of maximal drug-induced BRET by quinpirole \pm SEM.

Tr-FRET ligand binding

Materials: Spiperone-d₂, SNAP-Lumi4-Tb and 5x SNAP/CLIP labeling medium were purchased from Cisbio Bioassays. Eticlopride hydrochloride was purchased from Tocris Bioscience. Saponin was purchased from Fluka/Sigma-Aldrich. Bromocriptine, haloperidol, risperidone, spiperone, pluronic-F127,

Gpp(NH)p, DNA primers, Hanks Balanced Salt Solution H8264 (HBSS) and phosphate buffered saline (PBS) was purchased from Sigma-Aldrich.

Terbium cryptate labeling and membrane preparation

Terbium cryptate labeling of the SNAP-tagged receptors and membrane preparation was performed with minor changes to previously described methods (Klein Herenbrink *et al.*, 2016). Flp-In CHO-K1 cells stably expressing the mutant SNAP-D₂₅R constructs were grown in T175 flasks to approximately 90% confluency. Cell media was aspirated, and the cells were washed twice with 12 mL PBS. The cells were then incubated with terbium cryptate labeling reagent in 1xSNAP/CLIP labeling medium for 1 hr at in a humidified cell culture incubator with 5% CO₂ at 37°C. The terbium cryptate labeling reagent was then removed and the cells were washed once with 12 mL PBS. The labeled cells were then harvested in 10 mL PBS by cell scraping. Harvested cells were then collected by centrifugation at 300 g for 5 min and removal of the supernatant. The cell pellets were then frozen at –80°C for later membrane preparation. For cell membrane preparation, each cell pellet was removed from the –80°C freezer and thawed on ice. The pellet was then resuspended in 10 mL of ice-cold Buffer 1 (10mM HEPES 10 mM EDTA pH7.4). The pellet was then homogenised (IKA works T 10 basic Ultra-Turrax homogeniser) with eight bursts of 3 s on setting 4. The homogenized cells were transferred to an ultra-fast centrifuge tube and an additional 10 mL of Buffer one was added. The tube was then centrifuged at 48,000 g for 30 min at 4°C. The supernatant was discarded, 20 mL of Buffer one was added and the pellet was resuspended. The resuspension was then centrifuged a second time at 48,000 g for 30 min at 4°C. The supernatant was then removed, and the cell membrane pellet was collected by resuspension in 2 mL ice-cold Buffer 2 (10mM HEPES 0.1 mM EDTA pH 7.4). The resuspended membranes were then put through a syringe with a BD precision glide 26-gauge needle to make the solution uniform. Membrane protein concentration was determined by bicinchonic acid (BCA) assay detecting the absorbance at 562 nm on a CLARIOstar plate reader (BMG Labtech) using bovine serum albumin (BSA) as the protein standard. The cell membrane solution was then aliquoted and frozen at –80°C.

TR-FRET binding assay

All ligands were diluted in Binding Buffer (Hanks Balanced Salt Solution (Sigma H8264), 20 mM HEPES, 0.02% Pluronic-F127, 1% dimethyl sulfoxide, pH 7.4 (with KOH)). For competition binding experiments; 10 µL of spiperone-d2 in Binding Buffer was added to each well of a 384-well white optiplate LBS coated (PerkinElmer) at varied concentrations depending on the SNAP-D₂₅R mutant. 10 µL of increasing concentrations of unlabeled ligands were then added into the 10 µL of fluorescent ligand and mixed. A final concentration of 100 µM haloperidol was used to determine non-specific binding. Cell membranes were diluted to 0.075 µg/µL in Binding Buffer supplemented with 50 µg/mL saponin and 100 µM Gpp(NH)p.

TR-FRET measurements were acquired on a PHERAstar FS plate reader (BMG Labtech) at 37°C. The optiplate containing the ligand cocktails in the wells was incubated in the instrument for 6 min. The cell membrane solution was primed into the on-board injection system and incubated for 5 min. 20 µL of cell membrane solution was injected at 400 µL/s into the ligand cocktail wells to initiate the binding reaction. After 30-min incubation, the HTRF optic filter module was used to perform an excitation at 337 nm and simultaneous dual emission detection at 620 nm (terbium cryptate donor) and 665 nm (fluorescent ligand acceptor). The focal height was set to 10.4 mm. All experiments were performed in singlet wells. The TR-FRET binding values were determined by dividing the by the fluorescent ligand acceptor channel values by the terbium cryptate donor channel values and multiplying by 10,000. These values were then subtracted by the non-specific binding values determined in each experiment to give the specific HTRF ratio x 10,000. The data was then analysed with GraphPad Prism 8.2.1 using *Equations 1 and 2*.

Acknowledgements

Support for this research was provided by the National Institute on Drug Abuse–Intramural Research Program, Z1A DA000606-03 (LS), NIH grant MH54137 (JAJ) and National Health and Medical

Research Council (NHMRC) Project Grant APP1049564 (JRL). We thank Jackie Glenn for technical support in generating membrane preparations.

Additional information

Funding

Funder	Grant reference number	Author
National Institutes of Health	Z1A DA000606-03	Lei Shi
National Institutes of Health	MH54137	Jonathan A Javitch
National Health and Medical Research Council	APP1049564	J Robert Lane

The funders had no role in study design, data collection and interpretation, or the decision to submit the work for publication.

Author contributions

J Robert Lane, Conceptualization, Data curation, Formal analysis, Supervision, Funding acquisition, Investigation; Ara M Abramyan, Pramisha Adhikari, Ravi Kumar Verma, Herman D Lim, Hideaki Yano, Data curation, Formal analysis, Investigation; Alastair C Keen, Kuo-Hao Lee, Julie Sanchez, Formal analysis, Investigation; Jonathan A Javitch, Conceptualization, Investigation; Lei Shi, Conceptualization, Data curation, Formal analysis, Supervision, Funding acquisition, Investigation, Project administration

Author ORCIDs

Lei Shi  <https://orcid.org/0000-0002-4137-096X>

Decision letter and Author response

Decision letter <https://doi.org/10.7554/eLife.52189.sa1>

Author response <https://doi.org/10.7554/eLife.52189.sa2>

Additional files

Supplementary files

- Transparent reporting form

Data availability

All data generated or analysed during this study are included in the manuscript and supporting files.

References

- Abramyan AM, Quick M, Xue C, Javitch JA, Shi L. 2018. Exploring substrate binding in the extracellular vestibule of MhsT by atomistic simulations and markov models. *Journal of Chemical Information and Modeling* **58**:1244–1252. DOI: <https://doi.org/10.1021/acs.jcim.8b00175>, PMID: 29851339
- Amaro RE, Baudry J, Chodera J, Demir Ö, McCammon JA, Miao Y, Smith JC. 2018. Ensemble docking in drug discovery. *Biophysical Journal* **114**:2271–2278. DOI: <https://doi.org/10.1016/j.bpj.2018.02.038>, PMID: 29606412
- Ballesteros J, Weinstein H. 1995. Integrated methods for the construction of three-dimensional models of structure-function relations in G protein-coupled receptors. *Methods in Neurosciences* **25**:366–428. DOI: [https://doi.org/10.1016/S1043-9471\(05\)80049-7](https://doi.org/10.1016/S1043-9471(05)80049-7)
- Best RB, Zhu X, Shim J, Lopes PE, Mittal J, Feig M, Mackerell AD. 2012. Optimization of the additive CHARMM all-atom protein force field targeting improved sampling of the backbone ϕ , ψ and side-chain $\chi(1)$ and $\chi(2)$ dihedral angles. *Journal of Chemical Theory and Computation* **8**:3257–3273. DOI: <https://doi.org/10.1021/ct300400x>, PMID: 23341755
- Beuming T, Shi L. 2017. Editorial: computer aided Structure-based lead optimization. *Current Topics in Medicinal Chemistry* **17**:2575–2576. DOI: <https://doi.org/10.2174/156802661723170808161306>, PMID: 28889794

- Bonifazi A**, Yano H, Guerrero AM, Kumar V, Hoffman AF, Lupica CR, Shi L, Newman AH. 2019. Novel and potent dopamine D₂ Receptor Go-Protein Biased Agonists. *ACS Pharmacology & Translational Science* **2**:52–65. DOI: <https://doi.org/10.1021/acscptsci.8b00060>, PMID: 30775693
- Bradley P**, Misura KM, Baker D. 2005. Toward high-resolution de novo structure prediction for small proteins. *Science* **309**:1868–1871. DOI: <https://doi.org/10.1126/science.1113801>, PMID: 16166519
- Chien EY**, Liu W, Zhao Q, Katritch V, Han GW, Hanson MA, Shi L, Newman AH, Javitch JA, Cherezov V, Stevens RC. 2010. Structure of the human dopamine D3 receptor in complex with a D2/D3 selective antagonist. *Science* **330**:1091–1095. DOI: <https://doi.org/10.1126/science.1197410>, PMID: 21097933
- Congreve M**, Dias JM, Marshall FH. 2014. Structure-based drug design for G protein-coupled receptors. *Progress in Medicinal Chemistry* **53**:1–63. DOI: <https://doi.org/10.1016/B978-0-444-63380-4.00001-9>, PMID: 24418607
- Feller SE**, Zhang Y, Pastor RW, Brooks BR. 1995. Constant pressure molecular dynamics simulation: the langevin piston method. *The Journal of Chemical Physics* **103**:4613–4621. DOI: <https://doi.org/10.1063/1.470648>
- Free RB**, Chun LS, Moritz AE, Miller BN, Doyle TB, Conroy JL, Padron A, Meade JA, Xiao J, Hu X, Dulcey AE, Han Y, Duan L, Titus S, Bryant-Genevier M, Barnaeva E, Ferrer M, Javitch JA, Beuming T, Shi L, et al. 2014. Discovery and characterization of a G protein-biased agonist that inhibits β -arrestin recruitment to the D2 dopamine receptor. *Molecular Pharmacology* **86**:96–105. DOI: <https://doi.org/10.1124/mol.113.090563>, PMID: 24755247
- Hirose T**, Kikuchi T. 2005. Aripiprazole, a novel antipsychotic agent: dopamine D2 receptor partial agonist. *The Journal of Medical Investigation* **52**:284–290. DOI: <https://doi.org/10.2152/jmi.52.284>, PMID: 16366516
- Huang L**, Roux B. 2013. Automated force field parameterization for nonpolarizable and polarizable atomic models based on ab initio target data. *Journal of Chemical Theory and Computation* **9**:3543–3556. DOI: <https://doi.org/10.1021/ct4003477>
- Ioerger TR**, Du C, Linthicum DS. 1999. Conservation of cys-cys trp structural triads and their geometry in the protein domains of immunoglobulin superfamily members. *Molecular Immunology* **36**:373–386. DOI: [https://doi.org/10.1016/S0161-5890\(99\)00032-2](https://doi.org/10.1016/S0161-5890(99)00032-2), PMID: 10444001
- Javitch JA**, Shi L, Simpson MM, Chen J, Chiappa V, Visiers I, Weinstein H, Ballesteros JA. 2000. The fourth transmembrane segment of the dopamine D2 receptor: accessibility in the binding-site crevice and position in the transmembrane bundle. *Biochemistry* **39**:12190–12199. DOI: <https://doi.org/10.1021/bi001069m>, PMID: 11015197
- John B**, Sali A. 2003. Comparative protein structure modeling by iterative alignment, model building and model assessment. *Nucleic Acids Research* **31**:3982–3992. DOI: <https://doi.org/10.1093/nar/gkg460>, PMID: 12853614
- Kimura KT**, Asada H, Inoue A, Kadji FMN, Im D, Mori C, Arakawa T, Hirata K, Nomura Y, Nomura N, Aoki J, Iwata S, Shimamura T. 2019. Structures of the 5-HT2A receptor in complex with the antipsychotics risperidone and zotepine. *Nature Structural & Molecular Biology* **26**:121–128. DOI: <https://doi.org/10.1038/s41594-018-0180-z>
- Klauda JB**, Venable RM, Freites JA, O'Connor JW, Tobias DJ, Mondragon-Ramirez C, Vorobyov I, MacKerell AD, Pastor RW. 2010. Update of the CHARMM all-atom additive force field for lipids: validation on six lipid types. *The Journal of Physical Chemistry B* **114**:7830–7843. DOI: <https://doi.org/10.1021/jp101759q>, PMID: 20496934
- Klein Herenbrink C**, Sykes DA, Donthamsetti P, Canals M, Coudrat T, Shonberg J, Scammells PJ, Capuano B, Sexton PM, Charlton SJ, Javitch JA, Christopoulos A, Lane JR. 2016. The role of kinetic context in apparent biased agonism at GPCRs. *Nature Communications* **7**:10842. DOI: <https://doi.org/10.1038/ncomms10842>, PMID: 26905976
- Klein Herenbrink C**, Verma R, Lim HD, Kopinathan A, Keen A, Shonberg J, Draper-Joyce CJ, Scammells PJ, Christopoulos A, Javitch JA, Capuano B, Shi L, Lane JR. 2019. Molecular determinants of the intrinsic efficacy of the antipsychotic aripiprazole. *ACS Chemical Biology* **14**:1780–1792. DOI: <https://doi.org/10.1021/acscchembio.9b00342>, PMID: 31339684
- Latorraca NR**, Venkatakrishnan AJ, Dror RO. 2017. GPCR dynamics: structures in motion. *Chemical Reviews* **117**:139–155. DOI: <https://doi.org/10.1021/acs.chemrev.6b00177>, PMID: 27622975
- Liu W**, Chun E, Thompson AA, Chubukov P, Xu F, Katritch V, Han GW, Roth CB, Heitman LH, IJzerman AP, Cherezov V, Stevens RC. 2012. Structural basis for allosteric regulation of GPCRs by sodium ions. *Science* **337**:232–236. DOI: <https://doi.org/10.1126/science.1219218>, PMID: 22798613
- MacKerell AD**, Bashford D, Bellott M, Dunbrack RL, Evanseck JD, Field MJ, Fischer S, Gao J, Guo H, Ha S, Joseph-McCarthy D, Kuchnir L, Kuczera K, Lau FT, Mattos C, Michnick S, Ngo T, Nguyen DT, Prodhom B, Reiher WE, et al. 1998. All-atom empirical potential for molecular modeling and dynamics studies of proteins. *The Journal of Physical Chemistry B* **102**:3586–3616. DOI: <https://doi.org/10.1021/jp973084f>, PMID: 24889800
- MacKerell AD**, Feig M, Brooks CL. 2004. Improved treatment of the protein backbone in empirical force fields. *Journal of the American Chemical Society* **126**:698–699. DOI: <https://doi.org/10.1021/ja036959e>, PMID: 14733527
- Malinauskaitė L**, Quick M, Reinhard L, Lyons JA, Yano H, Javitch JA, Nissen P. 2014. A mechanism for intracellular release of Na⁺ by neurotransmitter/sodium symporters. *Nature Structural & Molecular Biology* **21**:1006–1012. DOI: <https://doi.org/10.1038/nsmb.2894>, PMID: 25282149
- Manglik A**, Lin H, Aryal DK, McCorvy JD, Dengler D, Corder G, Levit A, Kling RC, Bernat V, Hübner H, Huang X-P, Sassano MF, Giguère PM, Löber S, Duan Da, Scherrer G, Kobilka BK, Gmeiner P, Roth BL, Shoichet BK. 2016. Structure-based discovery of opioid analgesics with reduced side effects. *Nature* **537**:185–190. DOI: <https://doi.org/10.1038/nature19112>

- McCorvy JD**, Butler KV, Kelly B, Rechsteiner K, Karpiak J, Betz RM, Kormos BL, Shoichet BK, Dror RO, Jin J, Roth BL. 2018. Structure-inspired design of β -arrestin-biased ligands for aminergic GPCRs. *Nature Chemical Biology* **14**:126–134. DOI: <https://doi.org/10.1038/nchembio.2527>, PMID: 29227473
- McGibbon RT**, Beauchamp KA, Harrigan MP, Klein C, Swails JM, Hernández CX, Schwantes CR, Wang LP, Lane TJ, Pande VS. 2015. MDTraj: a modern open library for the analysis of molecular dynamics trajectories. *Biophysical Journal* **109**:1528–1532. DOI: <https://doi.org/10.1016/j.bpj.2015.08.015>, PMID: 26488642
- Michino M**, Donthamsetti P, Beuming T, Banala A, Duan L, Roux T, Han Y, Trinquet E, Newman AH, Javitch JA, Shi L. 2013. A single glycine in extracellular loop 1 is the critical determinant for pharmacological specificity of dopamine D2 and D3 receptors. *Molecular Pharmacology* **84**:854–864. DOI: <https://doi.org/10.1124/mol.113.087833>, PMID: 24061855
- Michino M**, Beuming T, Donthamsetti P, Newman AH, Javitch JA, Shi L. 2015a. What can crystal structures of aminergic receptors tell us about designing subtype-selective ligands? *Pharmacological Reviews* **67**:198–213. DOI: <https://doi.org/10.1124/pr.114.009944>, PMID: 25527701
- Michino M**, Free RB, Doyle TB, Sibley DR, Shi L. 2015b. Structural basis for Na^+ -sensitivity in dopamine D2 and D3 receptors. *Chemical Communications* **51**:8618–8621. DOI: <https://doi.org/10.1039/c5cc02204e>
- Michino M**, Boateng CA, Donthamsetti P, Yano H, Bakare OM, Bonifazi A, Ellenberger MP, Keck TM, Kumar V, Zhu C, Verma R, Deschamps JR, Javitch JA, Newman AH, Shi L. 2017. Toward understanding the structural basis of partial agonism at the dopamine D₃ Receptor. *Journal of Medicinal Chemistry* **60**:580–593. DOI: <https://doi.org/10.1021/acs.jmedchem.6b01148>, PMID: 27983845
- Neve KA**. 1991. Regulation of dopamine D2 receptors by sodium and pH. *Molecular Pharmacology* **39**:570–578. PMID: 2017157
- Newman AH**, Beuming T, Banala AK, Donthamsetti P, Pongetti K, LaBounty A, Levy B, Cao J, Michino M, Luedtke RR, Javitch JA, Shi L. 2012. Molecular determinants of selectivity and efficacy at the dopamine D3 receptor. *Journal of Medicinal Chemistry* **55**:6689–6699. DOI: <https://doi.org/10.1021/jm300482h>, PMID: 22632094
- Newton CL**, Wood MD, Strange PG. 2016. Examining the effects of sodium ions on the binding of antagonists to dopamine D2 and D3 receptors. *PLOS ONE* **11**:e0158808. DOI: <https://doi.org/10.1371/journal.pone.0158808>, PMID: 27379794
- Piana S**, Lindorff-Larsen K, Shaw DE. 2011. How robust are protein folding simulations with respect to force field parameterization? *Biophysical Journal* **100**:L47–L49. DOI: <https://doi.org/10.1016/j.bpj.2011.03.051>, PMID: 21539772
- Rasmussen SG**, Choi HJ, Fung JJ, Pardon E, Casarosa P, Chae PS, Devree BT, Rosenbaum DM, Thian FS, Kobilka TS, Schnapp A, Konetzki I, Sunahara RK, Gellman SH, Pautsch A, Steyaert J, Weis WI, Kobilka BK. 2011. Structure of a nanobody-stabilized active state of the $\beta(2)$ adrenoceptor. *Nature* **469**:175–180. DOI: <https://doi.org/10.1038/nature09648>, PMID: 21228869
- Roberts DJ**, Strange PG. 2005. Mechanisms of inverse agonist action at D2 dopamine receptors. *British Journal of Pharmacology* **145**:34–42. DOI: <https://doi.org/10.1038/sj.bjp.0706073>, PMID: 15735658
- Roos K**, Wu C, Damm W, Reboul M, Stevenson JM, Lu C, Dahlgren MK, Mondal S, Chen W, Wang L, Abel R, Friesner RA, Harder ED. 2019. OPLS3e: extending force field coverage for Drug-Like small molecules. *Journal of Chemical Theory and Computation* **15**:1863–1874. DOI: <https://doi.org/10.1021/acs.jctc.8b01026>, PMID: 30768902
- Roth BL**, Lopez E, Patel S, Kroeze WK. 2000. The multiplicity of serotonin receptors: uselessly diverse molecules or an embarrassment of riches? *The Neuroscientist* **6**:252–262. DOI: <https://doi.org/10.1177/107385840000600408>
- Scherer MK**, Trendelkamp-Schroer B, Paul F, Pérez-Hernández G, Hoffmann M, Plattner N, Wehmeyer C, Prinz JH, Noé F. 2015. PyEMMA 2: a software package for estimation, validation, and analysis of markov models. *Journal of Chemical Theory and Computation* **11**:5525–5542. DOI: <https://doi.org/10.1021/acs.jctc.5b00743>, PMID: 26574340
- Seeman P**. 2014. Clozapine, a fast-off-D2 antipsychotic. *ACS Chemical Neuroscience* **5**:24–29. DOI: <https://doi.org/10.1021/cn400189s>, PMID: 24219174
- Sherman W**, Day T, Jacobson MP, Friesner RA, Farid R. 2006. Novel procedure for modeling ligand/receptor induced fit effects. *Journal of Medicinal Chemistry* **49**:534–553. DOI: <https://doi.org/10.1021/jm050540c>, PMID: 16420040
- Shi L**, Javitch JA. 2004. The second extracellular loop of the dopamine D2 receptor lines the binding-site crevice. *PNAS* **101**:440–445. DOI: <https://doi.org/10.1073/pnas.2237265100>, PMID: 14704269
- Sibley DR**, Shi L. 2018. A new era of rationally designed antipsychotics. *Nature* **555**:170–172. DOI: <https://doi.org/10.1038/d41586-018-02328-z>, PMID: 29517027
- Silvestre JS**, Prous J. 2005. Research on adverse drug events. I. Muscarinic M3 receptor binding affinity could predict the risk of antipsychotics to induce type 2 diabetes. *Methods and Findings in Experimental and Clinical Pharmacology* **27**:289–304. DOI: <https://doi.org/10.1358/mf.2005.27.5.908643>
- Stolzenberg S**, Li Z, Quick M, Malinauskaitė L, Nissen P, Weinstein H, Javitch JA, Shi L. 2017. The role of transmembrane segment 5 (TM5) in Na^+ release and the conformational transition of neurotransmitter:sodium symporters toward the inward-open state. *Journal of Biological Chemistry* **292**:7372–7384. DOI: <https://doi.org/10.1074/jbc.M116.757153>
- Swope WC**, Pitera JW, Suits F. 2004. Describing Protein Folding Kinetics by Molecular Dynamics Simulations. 1. Theory [†]. *The Journal of Physical Chemistry B* **108**:6571–6581. DOI: <https://doi.org/10.1021/jp037421y>

- Sykes DA**, Moore H, Stott L, Holliday N, Javitch JA, Lane JR, Charlton SJ. 2017. Extrapyramidal side effects of antipsychotics are linked to their association kinetics at dopamine D2 receptors. *Nature Communications* **8**:763. DOI: <https://doi.org/10.1038/s41467-017-00716-z>
- Trendelkamp-Schroer B**, Noé F. 2013. Efficient bayesian estimation of markov model transition matrices with given stationary distribution. *The Journal of Chemical Physics* **138**:164113. DOI: <https://doi.org/10.1063/1.4801325>, PMID: 23635117
- Vanommeslaeghe K**, Hatcher E, Acharya C, Kundu S, Zhong S, Shim J, Darian E, Guvench O, Lopes P, Vorobyov I, Mackerell AD. 2010. CHARMM general force field: a force field for drug-like molecules compatible with the CHARMM all-atom additive biological force fields. *Journal of Computational Chemistry* **31**:671–690. DOI: <https://doi.org/10.1002/jcc.21367>, PMID: 19575467
- Venkatakrishnan AJ**, Deupi X, Lebon G, Tate CG, Schertler GF, Babu MM. 2013. Molecular signatures of G-protein-coupled receptors. *Nature* **494**:185–194. DOI: <https://doi.org/10.1038/nature11896>, PMID: 23407534
- Wang S**, Wacker D, Levit A, Che T, Betz RM, McCorvy JD, Venkatakrishnan AJ, Huang XP, Dror RO, Shoichet BK, Roth BL. 2017. D₄ dopamine receptor high-resolution structures enable the discovery of selective agonists. *Science* **358**:381–386. DOI: <https://doi.org/10.1126/science.aan5468>, PMID: 29051383
- Wang S**, Che T, Levit A, Shoichet BK, Wacker D, Roth BL. 2018. Structure of the D2 dopamine receptor bound to the atypical antipsychotic drug risperidone. *Nature* **555**:269–273. DOI: <https://doi.org/10.1038/nature25758>, PMID: 29466326
- Weis WI**, Kobilka BK. 2018. The molecular basis of G Protein-Coupled receptor activation. *Annual Review of Biochemistry* **87**:897–919. DOI: <https://doi.org/10.1146/annurev-biochem-060614-033910>, PMID: 29925258
- Zhang B**, Albaker A, Plouffe B, Lefebvre C, Tiberi M. 2014. Constitutive activities and inverse agonism in dopamine receptors. *Advances in Pharmacology* **70**:175–214. DOI: <https://doi.org/10.1016/B978-0-12-417197-8.00007-9>, PMID: 24931197